Memoirs of the Faculty of Engineering, Nagoya University
Vol. 30, No. 1. (1978)

THE LAMINAR AND TURBULENT BOUNDARY LAYERS ON SOME ROTATING BODIES IN AXIAL FLOWS

YOSHIMASA FURUYA*, IKUO NAKAMURA and SHINTARO YAMASHITA

Department of Mechanical Engineering

(Received May 30, 1978)

Abstract

Theories of the laminar boundary layers on spinning bodies of revolution and experiments on the turbulent boundary layers on various rotating bodies in axial flows with or without pressure gradients are presented. The laminar boundary layer theories concern with a rotating body of arbitrary shape in a uniform stream or in a quiescent fluid and with rotating thin cylinder in a uniform stream. For the first flow problem a universal series solution is obtained and also a universal series solution is calculated for the thermal boundary layer of the second problem. A higher order consideration is developed for the third flow. The acceleration phenomenon in the boundary layer induced by the rotation of a thin cylinder is clarified by use of a perturbation method.

The thick turbulent boundary layers on rotating cylinders with a ring or a step in a constant pressure flow are examined. The roughness element disturbs the velocity distribution in the turbulent boundary layer, especially in the meridional direction strongly. The velocity profile in the azimuthal direction is rather stable to such a disturbance. An expression of generalized quasi-collateral condition of the velocity distribution is obtained. The effect of pressure gradients on the turbulent boundary layer on a rotating cylinder is clarified in the final chapter. The imposed pressure gradients are adverse and favorable. The shear stress distribution in the peripheral direction is calculated and the existence of the constant moment layer is shown. A universal logarithmic velocity distribution law in the peripheral direction is established by use of a matching method. A role of a Richardson number as a representative of a character of this flow is discussed.

---

* Emeritus Professor, President of Gifu Technical College.

CONTENTS

I General Introduction

The problem of rotating fluids has attracted the attention of a considerable number of fluid dynamics researchers, who have analyzed their peculiar behaviors. Nevertheless, many features of the flow remain to be clarified. This report is concerned with the mechanics of the boundary layer on various axisymmetric rotating bodies in various types of axial flows. An assumption will be always made that the flow is rotationaly symmetric, so the Magnus or Robins effect is excluded. This boundary layer is influenced by factors which are absent in the plane boundary layer, that is, the effect of centrifugal force produced by rotation and the effect of transverse curvature.

In practical engineering problems, this boundary layer appears on a boss of axial flow turbo-machinery, on spinning projectiles, on a rotor of a generator and various other rotating machinery. The boundary layer is a special case of the general three-dimensional boundary layer, and the authors investigated this flow as an important step towards understanding the general three-dimensional boundary layer. In practice, the authors faced the difficult problem of the higher order effects, and the effects of roughness element of the boundary layer. Among the former, the transverse curvature and the centrifugal force are particularly interesting with respect to the so-called universal velocity distribution law, the law of the wall and the velocity defect law. These two factors affect the turbulent boundary layer in a complex manner. To make some contribution toward the establishing of a universal velocity distribution law of the boundary layer is one of the main objects of this research.

A first step in this area was made by Wieselsberger[1] who measured drag and torque in three types of rotating bodies in axial flow and indicated the strong influence of the rotation speed. After his research, various investigators took up the problem. Among them, the work of Schlichting[2], Parr[3], and the present authors[4] may be mentioned. Schlichting solved the problem of the laminar boundary layer on a spinning body in axial flow using the Kármán-Pohlhausen method. Parr measured for the first time the velocity profiles of this boundary layer and presented a simple relationship between the meridian velocity profile and azimuthal velocity profile. The authors measured the boundary layer in various cases and the results are presented in Ref. 4). Also other related references should be made to that paper[4].

Modern research has been concerned mainly with the turbulent structure and its calculation[5]~[12]. Cham & Head[5] considered entrainment of the boundary layer. A sophisticated calculation method for the turbulent boundary layer first appeared in this field was a paper of Koosinlin, Launder & Sharma[8]. They used an isotropic eddy viscosity model and compared the calculated results with the authors' experiment. Koosinlin & Lockwood[9] proposed a modification of the method. Related calculations have been put forth by Sharma[10] and Launder, Priddin & Sharma[11]. Turbulence measurements were made by Bissonnette & Mellor[6] and Lohmann[7]. The latter authors considered this problem as a case of rapid distortion of the turbulent flow and measured the flow which was developed on a stationary cylinder then disturbed by a coaxial rotating cylinder. Bissonnette & Mellor[6] showed that turbulence energy increased quickly as a response to the step type disturbance and

also that redistribution of the energy proceeded rapidly. Lohmann[7] measured the energy spectrum of the turbulence in the mean streamline direction and clarified that the large eddy was disrupted by the rotation, and that the strength of small scale eddy increased. All of these researches indicate the strong effect of centrifugal force on the structure of turbulence. A Richardson number recommended by Bradshaw[13] proved its usefulness in many papers.

In this comprehensive report of our research, the following problems will be discussed. In Chapter Ⅱ, laminar boundary layer problems will be solved using a series expansion in the case of thin boundary layer, and a solution will be obtained by use of the momentum integral method for the thick laminar boundary layer. A consideration will be made of the thermal boundary layer on a spinning body in a quiescent fluid. Considering their practical importance, experimental studies of turbulent boundary layers disturbed by a ring or a step on rotating cylinders in axial flow will be described in Chapter Ⅲ. The pressure gradient is one of the most important factors of the turbulent boundary layer, so the behavior of the turbulent boundary layer on a rotating cylinder under the influence of various pressure gradients will be examined in Chapter Ⅳ. A universal velocity distribution law will also be presented in the same chapter.

Ⅱ The Laminar Boundary Layer on a Spinning Body of Revolution

2. 1. Introduction

Laminar flow equations describing the boundary layer developing on a body of revolution spinning around its axis of symmetry were treated by many researchers. The salient feature of the flow is the effect of the centrifugal force acting on the fluid particle in the boundary layer. In some cases it shifts the separation point and the transition point. In this chapter three problems will be discussed: first, the steady laminar boundary layer on a rotating blunt body in axial flow, second, the thermal boundary layer on a rotating body in a quiescent fluid, and third, the thick laminar boundary layer on a rotating thin cylinder.

Theoretical considerations were presented by Miss D. M. Hannah[14], Schlichting[2], Parr[3], Rittmann[15], and Muraca[16] on the first problem. Related unsteady problems were treated by Illingworth[17],[18] and others[19],[20]. Concerning to the second problems, references should be made to Eox[21], Dorfman & Serazedinov[22], Banks[23], and Manohar[24]. About third problem, there is no published work within authors' knowledge, but studies on the flow on a thin needle without spin are numerous, for example, theories of Seban & Bond[25], Glauert & Lighthill[26], Stewartson[27] and others[28]~[32] should be mentioned.

2. 2. Blunt body

2. 2. 1. The laminar boundary layer on a spinning body of arbitrary shape in axial flow

Introductory remarks With steady axisymmetrical flow past a blunt nose body of revolution the laminar boundary layer equations can be reduced to non-dimensional forms which have no universal characteristic parameter such as Reynolds number, and the same is true for the case of a rotating body in an infinite fluid at rest.

On the other hand, the boundary layer on a spinning body in axial flow depends on a parameter Ω defined in Eq. (2.2) which represents the effect of the meridian component of the centrifugal force produced by rotation. In the present section, the solution is expanded in terms of the meridian coordinate and the functional coefficients of the series are determined by the sequence of simultaneous ordinary differential equations. It is shown that these functional coefficients can be split into the universal functions which depend only on the parameter Ω but depend neither on the shape of the body nor on the main flow. That is, two Blasius-Howarth series are obtained.

Current methods for the boundary layer equations are mainly finite difference or finite element calculations, but since the series solutions are still important for its theoretical clarity and simplicity, then the authors considered the problems of Chapter Ⅱ using series expansions.

Basic equations and the method of solution With x as the distance measured along the meridian curve of the body from the foward stagnation point, z as the distance from the surface, U and W as the corresponding velocities, V as the azimuthal velocity component, U_e as the main stream velocity, R as the radius of the body, ω and ν as the angular velocity of the body and kinematic viscosity respectively, the basic equations and the boundary conditions of steady incompressible laminar boundary layer of the problem are in non-dimensional form,

$$\left.\begin{aligned} &G\partial_{\eta\eta\eta}f+\frac{1}{2}\{\partial_{\eta\eta}f\partial_{\xi}(Gf)-G\partial_{\eta}f\partial_{\xi\eta}f+\Omega^2g^2G'+GFF'\}=0,\\ &G\partial_{\eta\eta}g+\frac{1}{2}\{\partial_{\eta}g\partial_{\xi}(Gf)-\partial_{\eta}f\partial_{\xi}(Gg)\}=0,\\ &\eta=0:f=\partial_{\eta}f=0,\ g=G,\\ &\eta\to\infty:\partial_{\eta}f\to F,\ g\to 0, \end{aligned}\right\} \tag{2.1}$$

where

$$\left.\begin{aligned} &U=\partial_z\Psi,\ W=-\partial_x\Psi-\Psi R'/R,\\ &\xi=x/R_m,\ \eta=\sqrt{2U_m/\nu R_m}\,z,\ \Omega=R_m\omega/U_m,\\ &f(\xi,\eta)=\sqrt{2/\nu R_mU_m}\,\Psi,\ g(\xi,\eta)=V/R_m\omega, \end{aligned}\right\} \tag{2.2}$$

and

$$F(\xi)=U_e/U_m,\ G(\xi)=R/R_m,$$

where U_m and R_m are the representative values of U_e and R respectively.

Let the blunt body contour and the velocity of main flow be expressed by the series

$$\left.\begin{aligned} G(\xi)&=\xi+\alpha_3\xi^3+\alpha_5\xi^5+\alpha_7\xi^7+\cdots,\\ F(\xi)&=\xi+\beta_3\xi^3+\beta_5\xi^5+\beta_7\xi^7+\cdots, \end{aligned}\right\} \tag{2.3}$$

respectively. We put the series solution of Eq. (2.1) as follows:

$$\left.\begin{aligned} f(\xi,\ \eta) &= f_1\xi + 2\beta_3 f_3\xi^3 + 3\beta_5 f_5\xi^5 + 4\beta_7 f_7\xi^7 + \cdots, \\ \text{and} \qquad & \\ g(\xi,\ \eta) &= g_1\xi + 2\alpha_3 g_3\xi^3 + 3\alpha_5 g_5\xi^5 + 4\alpha_7 g_7\xi^7 + , \end{aligned}\right\} \tag{2.4}$$

where f_1, g_1, f_3, g_3, $\cdots$ depend only on η. Substitution of these expressions into Eq. (2.1) yields a sequence of ordinary differential equations. The first set is Hannah's equation that is,

$$\left.\begin{aligned} & f_1''' = -f_1 f_1'' + \frac{1}{2}(f_1'^2 - 1) - \frac{1}{2}\Omega^2 g_1^2, \\ & g_1'' = -f_1 g_1' + f_1' g_1, \\ & \eta = 0 : f_1 = f_1' = 0,\ g_1 = 1, \\ & \eta \to \infty : f_1' \to 1,\ g_1 \to 0. \end{aligned}\right\} \tag{2.5}$$

General terms have the following forms:

$$\left.\begin{aligned} f'''_{2n-1} = \frac{1}{n\beta_{2n-1}}\Bigg[& -\sum_{i=1}^{n-1} i\alpha_{2n+1-2i}\beta_{2i-1} f'''_{2i-1} + \sum_{i=1}^{n}\left\{\sum_{j=1}^{n+1-i}\alpha_{2n+3-2(i+j)}\left(\frac{\beta_{2i-1}\beta_{2j-1}}{2}\right.\right. \\ & \times [ij\{-2(n+1-i)f''_{2i-1}f_{2j-1} + (2i-1)f'_{2i-1}f'_{2j-1}\} - (2i-1)] \\ & \left.\left. - \Omega^2\frac{\alpha_{2i-1}\alpha_{2j-1}}{2} ij\{2n+3-2(i+j)\} g_{2i-1}g_{2j-1}\right)\right\}\Bigg], \\ \text{and} \qquad & \\ g''_{2n-1} = \frac{1}{n\alpha_{2n-1}}\Bigg(& -\sum_{i=1}^{n-1} i\alpha_{2n+1-2i}\alpha_{2i-1} g''_{2i-1} + \sum_{i=1}^{n}\left[\sum_{j=1}^{n+1-i} ij\alpha_{2i-1}\beta_{2j-1}\alpha_{2n+3-2(i+j)}\right. \\ & \left.\times\{-(n+1-i)f_{2j-1}g'_{2i-1} + (n+1-j)f'_{2j-1}g_{2i-1}\}\right]\Bigg), \end{aligned}\right\} \tag{2.6}$$

while the boundary conditions are

$$\left.\begin{aligned} & \eta = 0 : f_{2n-1} = f'_{2n-1} = 0,\ g_{2n-1} = \frac{1}{n}, \\ & \eta \to \infty : f'_{2n-1} \to \frac{1}{n},\ g_{2n-1} \to 0, \\ \text{where} \qquad & \\ & n \geqq 2,\ \alpha_1 = \beta_1 = 1. \end{aligned}\right\} \tag{2.7}$$

It is possible to construct a recursive computer program for numerical calculation of Eq. (2.6) without obtaining the expanded each equations of Eq. (2.6) by hand. But the authors found that the numerical accuracy obtained by such a program was poorer than that of the numerical results of the following method.

If we consider the linearity of Eq. (2.6), we can split the functions f_3, f_5, $\cdots$, g_3, g_5, $\cdots$, using general function as the same way as for the case of the stationary

body, to obtain

$$\left.\begin{aligned}
&f_3=f_{3,1}+f_{3,2}\alpha_3/\beta_3, \quad g_3=g_{3,1}+g_{3,2}\beta_3/\alpha_3,\\
&f_5=f_{5,1}+f_{5,2}\alpha_5/\beta_5+f_{5,3}\beta_3^2/\beta_5+f_{5,4}\alpha_3\beta_3/\beta_5+f_{5,5}\alpha_3^2/\beta_5,\\
&g_5=g_{5,1}+g_{5,2}\beta_5/\alpha_5+g_{5,3}\beta_3^2/\alpha_5+g_{5,4}\alpha_3\beta_3/\alpha_5+g_{5,5}\alpha_3^2/\alpha_5,\\
&f_7=f_{7,1}+f_{7,2}\alpha_7/\beta_7+f_{7,3}\alpha_3^2\beta_3/\beta_7+f_{7,4}\beta_3^3/\beta_7+f_{7,5}\alpha_5\beta_3/\beta_7\\
&\qquad+f_{7,6}\beta_3\beta_5/\beta_7+f_{7,7}\alpha_3^3/\beta_7+f_{7,8}\alpha_3\alpha_5/\beta_7+f_{7,9}\alpha_3\beta_3^2/\beta_7\\
&\qquad+f_{7,10}\alpha_3\beta_5/\beta_7,\\
&g_7=g_{7,1}+g_{7,2}\beta_7/\alpha_7+g_{7,3}\alpha_3^2\beta_3/\alpha_7+g_{7,4}\beta_3^3/\alpha_7+g_{7,5}\alpha_5\beta_3/\alpha_7\\
&\qquad+g_{7,6}\beta_3\beta_5/\alpha_7+g_{7,7}\alpha_3^3/\alpha_7+g_{7,8}\alpha_3\alpha_5/\alpha_7+g_{7,9}\alpha_3\beta_3^2/\alpha_7\\
&\qquad+g_{7,10}\alpha_3\beta_5/\alpha_7.
\end{aligned}\right\} \tag{2.8}$$

The simultaneous differential equations and the boundary conditions which determine these functions are, for example, describing those for $f_{3,1}$, $g_{3,1}$:

$$\left.\begin{aligned}
&f_{3,1}'''=F[f_{3,1}]-1-\Omega^2 g_1 g_{3,2},\\
&g_{3,2}''=G[g_{3,2}, f_{3,1}],
\end{aligned}\right\} \tag{2.9}$$

$$\left.\begin{aligned}
&f_{3,2}'''=F[f_{3,2}]-\frac{1}{2}f_1 f_1''-\Omega^2\left(g_1 g_{3,1}+\frac{1}{2}g_1^2\right),\\
&g_{3,1}''=G[g_{3,1}, f_{3,2}]-\frac{1}{2}(f_1 g_1'-f_1' g_1),
\end{aligned}\right\} \tag{2.10}$$

$$\left.\begin{aligned}
&\eta=0: f_{3,1}=f_{3,1}'=f_{3,2}=f_{3,2}'=g_{3,2}=0,\ g_{3,1}=\frac{1}{2},\\
&\eta\to\infty: f_{3,1}'\to\frac{1}{2},\ f_{3,2}'=g_{3,2}=g_{3,1}\to 0,
\end{aligned}\right\} \tag{2.11}$$

where

$$F[f_{3,i}]=-f_1 f_{3,i}''+2(f_1' f_{3,i}'-f_1'' f_{3,i}), \tag{2.12}$$

and

$$G[g_{3,i}, f_{3,j}]=-f_1 g_{3,i}'+2f_1' g_{3,i}+g_1 f_{3,j}'-2g_1' f_{3,j}. \tag{2.13}$$

The equations for other general functions are presented in Ref. 33). These general functions do not depend on the coefficients α_{2i-1}, β_{2i-1} which specify the particular problem, but depend on Ω.

Results of calculations The numerical solution of Eq. (2.5) constitutes a nonlinear boundary value problem, so the method of Nachtsheim & Swigert[34] was employed. The method uses a Newton-Raphson iteration scheme to reduce the

problem into an initial value one. To perform the iteration, the auxiliary differential equations derived from the equation in question are calculated simultaneously. Value of η_e which must be used in the calculation instead of actual boundary, that is infinity, was taken as 10 and it was found by calculation reasonably far from the wall. Another set of equations, for $f_{i,j}$, $g_{i,j}$, are linear and the two point boundary value problem can be easily solved in principle by performing the calculation three times for three inferred initial values. It was found, however, that to get the accuracy of calculation the inferred value had to nearly coincide with the correct value. All the calculations were performed with a step size of 0.005 and double precision in computer. The outer limit of the boundary layer for the numerical calculation was taken as 10. The method of integration was Adams-Moulton.

Since the number of universal functions of this problem is large compared with the number of functions for the stationary case and they have parameter Ω, the values of the derivatives of these functions at the wall are tabulated in Ref. 33).

Application and discussion The separation point of laminar flow appears downstream of the shoulder of a sphere, if the main flow is expressed by the potential flow as is well known. In this case rotation moves the separation point forward to the shoulder and this phenomenon was surveyed by Hoskin[35]. On the other hand, experiment shows the laminar separation occurs upstream of the equater of the sphere. It is expected, in this case, that the rotation displaces the separation point in the downstream direction. Now we will investigate this phenomenon using Fage's date on a stationary sphere in a uniform stream.

According to Tomotika & Imai[36], Fage's date can be expressed as follows:

$$F(\xi)=\xi-0.2914\xi^3+0.0987\xi^5-0.0282\xi^7,\quad 0\leqq\xi\leqq 1.48. \tag{2.14}$$

Velocity distributions in the boundary layer based on this main flow velocity are presented in Fig. 2. 1 and 2. 2. In Fig. 2. 1, it is clearly seen that the parameter Ω affects the meridional velocity distribution more than the azimuthal velocity distribution. Figure 2. 2 shows the velocity distribution at the separation point θ_s

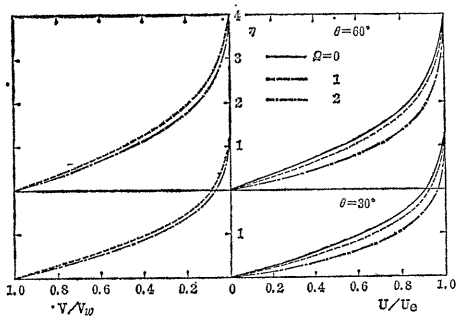

Fig. 2. 1. Velocity distribution on a rotating sphere using Fage's main flow. θ is meridional angle measured from the foward stagnation point. U_e: main flow velocity, V_w: azimuthal velocity of the body surface.

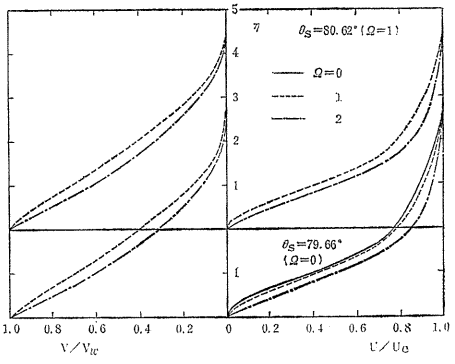

Fig. 2. 2. Velocity distribution at the separation point θ_s.

with both $\Omega=0$ and $\Omega=1$. Profiles in the meridional direction U/U_e show that rotation moves the separation point in the downstream direction. Figures 2. 3 and 2. 4 show polar plots of the velocity distributions in Figs. 2. 1 and 2. 2 respectively.

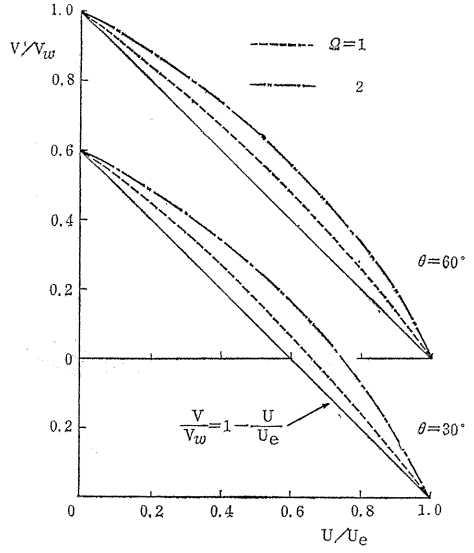

Fig. 2. 3. Polar plots, where $V/V_w=1-U/U_e$ represents the quasi-collateral velocity distribution.

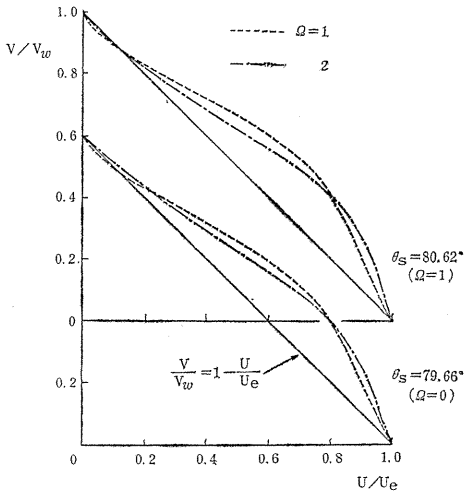

Fig. 2. 4. Variation of polar plots with Ω at the each separation point of $\Omega=0$ and $\Omega=1$ respectively.

Apparently, the quasi-collateral condition is violated especially at the separation point. The movement of the separation point with increasing value of Ω is presented in Fig. 2. 5. Although at the separation point, in due course we see that $(\partial_{\eta\eta}f)_{\eta=0}=0$, note that $(\partial_\eta g)_{\eta=0}$ does not vanish there, which can be seen in Fig. 2. 2. The shift of the separation point in the downstream direction was reported by Luthander & Rydberg[3 7] in early days by use of flow visualization using smoke, but since they did not measure the main flow velocity and their determination of the separation point does not seem sufficiently accurate, a comparison with this calculation can not be made. The present authors reported also the same phenomenon in the case of a rotating cylinder with a hemispherical cap in a duct[4], but the body shape and the pressure distribution on the body surface can not be expressed sufficiently well by Eq. (2. 3) within ξ^7 to the junction between the cap and the cylinder.

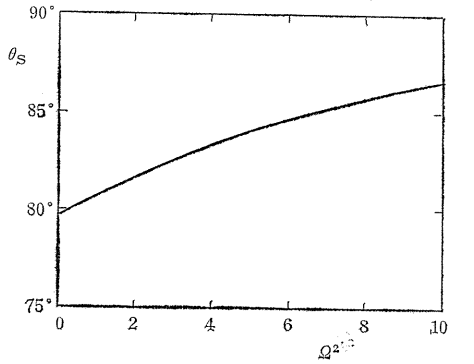

Fig. 2. 5. Shift of the separation point on a rotating sphere with increasing value of Ω^2.

Another peculiar velocity distribution observed on this rotating body at the high value of Ω is shown in Figs. 2. 6 - 2. 8[50]. In this case, a maximum of the meridian velocity component appears in the boundary layer. With the present method, this profile can not be predicted. Muraca's numerical results[16] should be mentioned with respect to the profile.

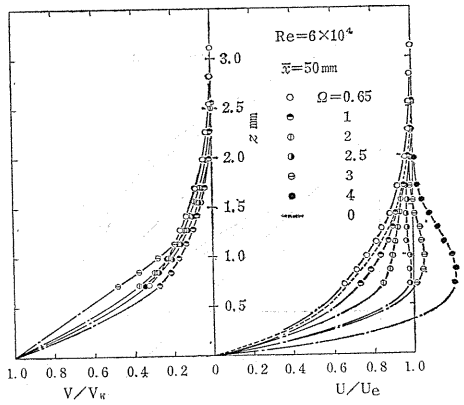

Fig. 2. 6. Velocity profiles on the hemispherical nose at high Ω at $\bar{x}$=50mm.

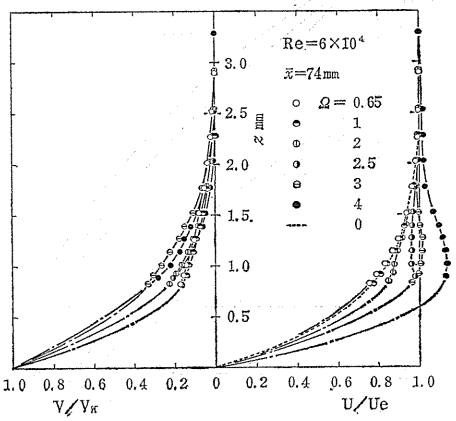

Fig. 2. 7. Velocity profiles on the hemispherical nose at high Ω at $\bar{x}$=74mm.

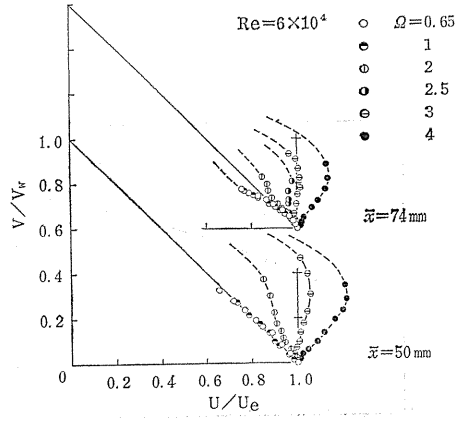

Fig. 2. 8. Polar plots of velocity distribution on the hemispherical nose at high Ω.

2. 2. 2. The thermal boundary layer on a spinning body of arbitrary shape in an infinite quiescent fluid

Introductory remarks Heat transfer by convection to or from a body of revolution spinning around its axis of symmetry in an otherwise undisturbed fluid has been investigated by many authors for its practical importance[38), 39)]. This problem can be classified into two categories according to the body shape. The first type has similar solution and the typical one is well known Kármán's rotating plate. The second type has no similar solution and the typical case is a rotating sphere and its boundary layer character has been a controversial problem[40)~42)]. In this

section, we treat the thermal boundary layer on a spinning body of revolution using similar method described in 2. 2. 1.

Basic equations and method of solution The coordinate system used is the same one appearing in 2. 2. 1. Using non-dimensional quantities we obtain following equations and boundary conditions for the velocity boundary layer:

$$\left.\begin{aligned} &G\partial_{\eta\eta\eta}f+\frac{1}{2}\{\partial_{\eta\eta}f\partial_{\xi}(Gf)-G\partial_{\eta}f\partial_{\xi\eta}f+G'g^2\}=0,\\ &G\partial_{\eta\eta}g+\frac{1}{2}\{\partial_{\eta}g\partial_{\xi}(Gf)-\partial_{\eta}f\partial_{\xi}(Gg)\}=0,\\ &\eta=0:f=\partial_{\eta}f=0,\ g=G,\\ &\eta\to\infty:\partial_{\eta}f\to 0,\ g\to 0, \end{aligned}\right\} \tag{2.15}$$

where

$$\left.\begin{aligned} &U=\partial_z\Psi,\ W=-\partial_x\Psi-\Psi R'/R,\ \xi=x/R_m,\ \eta=\sqrt{2\alpha_1\omega/\nu}\,z,\\ &\Psi=\sqrt{\nu\alpha_1\omega/2}\,R_m f(\xi,\ \eta),\quad V=R_m\alpha_1\omega g(\xi,\ \eta), \end{aligned}\right\} \tag{2.16}$$

and ω is the angular velocity of the body. The body contour is assumed as follows:

$$R/R_m=\alpha_1 G(\xi)=\alpha_1(\xi+\alpha_3\xi^3+\alpha_5\xi^5+\alpha_7\xi^7+\cdots). \tag{2.17}$$

From above equations, we can obtain following Blasius-Howarth series solutions which have no parameter such as Ω appearing in the problem of a spinning body in axial flow:

$$\left.\begin{aligned} U=\omega R_m\alpha_1\{&f'_1\xi+\alpha_3 f'_3\xi^3+\alpha_5(f'_{5,1}+f'_{5,2}\alpha_3^2/\alpha_5)\xi^5\\ &+\alpha_7(f'_{7,1}+f'_{7,2}\alpha_3^3/\alpha_7+f'_{7,3}\alpha_3\alpha_5/\alpha_7)\xi^7+\cdots\},\\ V=\omega R_m\alpha_1\{&g_1\xi+\alpha_3 g_3\xi^3+\alpha_5(g_{5,1}+g_{5,2}\alpha_3^2/\alpha_5)\xi^5\\ &+\alpha_7(g_{7,1}+g_{7,2}\alpha_3^3/\alpha_7+g_{7,3}\alpha_3\alpha_5/\alpha_7)\xi^7+\cdots\}. \end{aligned}\right\} \tag{2.18}$$

This type of solution was obtained by Fox[21] who used Stokes stream function but we employ other type of presentation as expressed first equation of Eq. (2.16) which corresponds to the method in 2. 2. 1.

Considering above results, we will seek the series solution of thermal boundary layer equation of this flow. Fundamental assumptions are as follows; the fluid is incompressible and has constant properties, wall temperature T_w is constant, and the bouyancy force and dissipation can be neglected. Then the basic non-dimensional energy equation and boundary conditions are

$$\left.\begin{aligned} &G\partial_{\eta\eta}\theta+\frac{P_r}{2}\{\partial_{\eta}\theta\partial_{\xi}(Gf)-G\partial_{\eta}f\partial_{\xi}\theta\}=0,\\ &\eta=0:\theta=1;\ \eta\to\infty:\theta\to 0, \end{aligned}\right\}$$

where

$$\theta=(T-T_\infty)/(T_w-T_\infty),\ P_r:\text{Prandtl number.} \tag{2.19}$$

We assume the series solution of Eq. (2.19) as follows:

$$\theta=\theta_1+\alpha_3\theta_3\xi^2+\alpha_5\theta_5\xi^4+\alpha_7\theta_7\xi^6+\cdots, \tag{2.20}$$

where θ_n is a function of η only. Equations for θ_1 and θ_3 are

$$\theta_1''=-P_rf_1\theta_1',\quad \theta_3''=P_r\{-f_1\theta_3'+f_1'\theta_3-(f_1+2f_3)\theta_1'\}. \tag{2.21}$$

Boundary conditions for them are

$$\eta=0:\theta_1=1,\ \theta_3=0;\ \eta\to\infty:\theta_1\to0,\ \theta_3\to0. \tag{2.22}$$

Since f_1 and f_3 are universal function, θ_1 and θ_3 depend only on Prandtl number but do not depend on the shape of the spinning body and the angular velocity. Equations correpond to θ_5 and θ_7 can also be split into universal functions, that is,

$$\theta_5=\theta_{5,1}+\theta_{5,2}\alpha_3^2/\alpha_5,\quad \theta_7=\theta_{7,1}+\theta_{7,2}\alpha_3^3/\alpha_7+\theta_{7,3}\alpha_3\alpha_5/\alpha_7. \tag{2.23}$$

Differential equations for these functions are

$$\left.\begin{aligned}\theta_{5,1}''&=P_r\{-f_1\theta_{5,1}'+2f_1'\theta_{5,1}-(2f_1+3f_{5,1})\theta_1'\},\\ \theta_{5,2}''&=P_r\{-f_1\theta_{5,2}'+2f_1'\theta_{5,2}+(f_1-f_3-3f_{5,2})\theta_1'+f_3'\theta_3-(f_1+2f_3)\theta_3'\},\end{aligned}\right\} \tag{2.24}$$

$$\left.\begin{aligned}\theta_{7,1}''&=P_r\{-f_1\theta_{7,1}'+3f_1'\theta_{7,1}-(3f_1+4f_{7,1})\theta_1'\},\\ \theta_{7,2}''&=P_r\{-f_1\theta_{7,2}'+3f_1'\theta_{7,2}-(f_1-f_3+f_{5,2}+4f_{7,2})\theta_1'+f_{5,2}'\theta_3\\ &\quad+(f_1-f_3-3f_{5,2})\theta_3'+2f_3'\theta_{5,2}-(f_1+2f_3)\theta_{5,2}'\},\\ \theta_{7,3}''&=P_r\{-f_1\theta_{7,3}'+3f_1'\theta_{7,3}+(3f_1-2f_3-f_{5,1}-4f_{7,3})\theta_1'+f_{5,1}'\theta_3\\ &\quad-(2f_1+3f_{5,1})\theta_3'+2f_3'\theta_{5,1}-(f_1+2f_3)\theta_{5,1}'\}.\end{aligned}\right\} \tag{2.25}$$

Boundary conditions are as follows:

$$\eta=0:\theta_{i,j}=0;\quad \eta\to\infty:\theta_{i,j}\to0. \tag{2.26}$$

Results Above equations also constitute a two point boundary value problem and the values of $f''_1(0)$ and $g'_1(0)$ are most difficult to find out. We used the values

Table 2. 1. Values of derivatives of universal functions $f_{i,j}$ and $g_{i,j}$ at the wall.

$f''_{1}(0)$	$g'_{1}(0)$	f''_{3}	g'_{3}	$f''_{5,1}$	$g'_{5,1}$	$f''_{5,2}$
0.360789	−0.435523	0.938835	−1.050668	1.34870	−1.40879	0.12259
$g'_{5,1}$	$f''_{7,1}$	$g'_{7,1}$	$f''_{7,2}$	$g'_{7,2}$	$f''_{7,3}$	$g'_{7,3}$
−0.23132	1.75781	−1.73806	0.19345	−0.07340	0.06652	−0.43039

Table 2. 2. Values of derivatives of θ_i at the wall.

Pr	$\theta'_1(0)$	θ'_3	$\theta'_{5,1}$	$\theta'_{5,2}$	$\theta'_{7,1}$	$\theta'_{7,2}$	$\theta'_{7,3}$
0.7	−0.228491	−0.265690	−0.388129	0.149876	−0.49966	−0.21872	0.47044
1.0	−0.280191	−0.328401	−0.482385	0.188050	−0.62326	−0.27566	0.59246
3.0	−0.482658	−0.576807	−0.858243	0.340484	−1.11889	−0.50308	1.08170

of Rogers & Lance[43] who solved Kármán's rotating flat plate. Other equations are linear and they can be solved by the same method described in 2. 2. 1. The values for the calculation of torque and heat transfer are tabulated in Tables 2. 1 and 2. 2. As an example, our results are compared with Bank's solution[23] which is applicable only for the sphere. The results showed excellent agreement.

2. 3. The thick laminar boundary layer on a rotating thin cylinder in axial flow

2. 3. 1. Introductory remarks

The problem of the laminar boundary layer on a stationary thin cylinder in axial flow has been investigated several times. For example, the solution of Seban & Bond[25] using an expansion from the leading edge, Glauert & Lighthill's solution of Pohlhausen method[26] and Jaffe & Okamura's numerical result[30] are known. In the case of supersonic flow it was analyzed by Gersten & Gross using the method of matched asymptotic expansions[32]. In this section a solution is presented for the laminar boundary layer flow on a rotating cylinder in axial uniform flow which is affected both effects of centrifugal force and transverse curvature. The method is based on the Glauert-Lighthill's momentum integral solution for the cylinder without rotation and extends it by a perturbation with respect of the ratio of circumferential velocity to uniform axial velocity. The results obtained show the effect of rotation on skin friction. It should be mentioned that according to Rao's construction of the law of the wall of the turbulent boundary layer on a thin cylinder[44], the laminar flow solution has a fundamental significance to establish the law of the wall of this type of the boundary layer.

2. 3. 2. Basic equations and the method of solution

Using the coordinate system shown in Fig. 2. 9, the boundary layer equations taking into account the effects of transverse curvature and rotation are

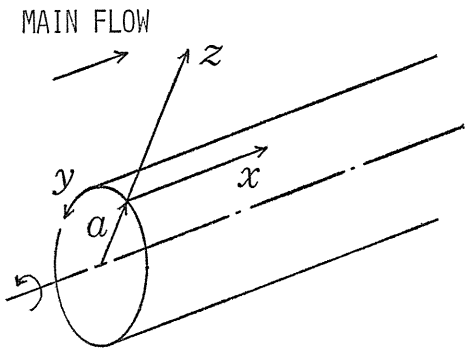

Fig. 2. 9. Coordinate system.

$$\left.\begin{aligned} &\partial_x U+\partial_z W+W/(a+z)=0,\\ &U\partial_x U+W\partial_z U=-\partial_x P/\rho+\nu\{\partial_{zz}U+\partial_z U/(a+z)\},\\ &U\partial_x V+W\partial_z V+VW/(a+z)=\nu\{\partial_{zz}V+\partial_z V/(a+z)-V/(a+z)^2\},\\ &V^2/(a+z)=\partial_z P/\rho. \end{aligned}\right\} \quad (2.27)$$

Boundary conditions are

$$\left.\begin{aligned} &z=0 : U=W=0,\ V=V_w,\\ &z\to\infty : U\to U_e,\ V\to 0. \end{aligned}\right\} \quad (2.28)$$

A fundamental parameter of this problem is the speed ratio Ω, that is,

$$\Omega=V_w/U_e,$$

where V_w is the circumferential velocity of the cylinder and U_e is the external velocity.

We assume that the solution can be expanded with respect to Ω, that is,

$$\left.\begin{aligned} &U=U_0+\Omega^2U_2+\cdots,\ V=\Omega V_1+\Omega^3V_3+\cdots,\\ &W=W_0+\Omega^2W_2+\cdots,\ P=P_0+\Omega^2P_2+\cdots. \end{aligned}\right\} \quad (2.29)$$

Of course Ω is assumed to be a small parameter. Using these expansions and Eq. (2.27), we obtain the following system of equations:

$$\left.\begin{aligned} &\partial_x U_0+\partial_z W_0+W_0/(a+z)=0,\\ &U_0\partial_x U_0+W_0\partial_z U_0=\nu\{\partial_{zz}U_0+\partial_z U_0/(a+z)\}, \end{aligned}\right\} \quad (2.30)$$

$$U_0\partial_x V_1+W_0\partial_z V_1+V_1W_0/(a+z)=\nu\{\partial_{zz}V_1+\partial_z V_1/(a+z)-V_1/(a+z)^2\}, \quad (2.31)$$

$$\left.\begin{aligned} &\partial_x U_2+\partial_z W_2+W_2/(a+z)=0,\\ &\partial_x(U_0U_2)+W_0\partial_z U_2+W_2\partial_z U_0=-\partial_x P_2/\rho+\nu\{\partial_{zz}U_2+\partial_z U_2/(a+z)\},\\ &V_1^2/(a+z)=\partial_z P_2/\rho, \end{aligned}\right\} \quad (2.32)$$

$$\cdots\cdots\cdots\cdots\cdots\cdots$$

$$\cdots\cdots\cdots\cdots\cdots\cdots.$$

Boundary conditions are

$$\left.\begin{aligned} &z=0 : U_0=U_2=\cdots=0,\quad W_0=W_2=\cdots=0,\\ &\qquad V_1=U_e,\quad V_3=\cdots=0,\\ &z\to\infty : U_0\to U_e,\ U_2,\ \cdots\to 0,\quad V_1,\ V_3,\ \cdots\to 0. \end{aligned}\right\} \quad (2.33)$$

Equation (2.30) corresponds to the non-rotating cylinder in axial flow and has the

momentum integral solution obtained by Glauert & Lighthill. They assumed a velocity distribution including an unknown parameter α_0 as follows:

$$\left.\begin{aligned} U_0 &= \begin{cases} U_e\alpha_0^{-1}\ln(1+\zeta)\ ;\ (\zeta \leqq \zeta_0 = e^{\alpha_0}-1), \\ U_e \qquad\qquad\ ;\ (\zeta \geqq \zeta_0), \end{cases} \\ \zeta &= z/a, \end{aligned}\right\} \tag{2.34}$$

where $\zeta_0=\delta_{x0}/a$ and a boundary layer thickness δ_{x0} is determined by the condition

$$\delta_{x0}=[z]_{U_0=U_e}.$$

Contribution of U_0 to the wall shear stress in the x-direction is

$$\tau_{x0}=\mu[\partial_z U_0]_{z=0}=\mu U_e/a\alpha_0. \tag{2.35}$$

The zeroth order momentum integral equation and its solution are

$$d\alpha_0/d\hat{\xi}=\alpha_0^2/\{(2-3\alpha_0+2\alpha_0^2)e^{2\alpha_0}-(2+\alpha_0)\}, \tag{2.36}$$

$$\hat{\xi}=e^{2\alpha_0}+3-2\alpha_0^{-1}(e^{2\alpha_0}-1)+\int_0^{2\alpha_0}(e^t-1)t^{-1}dt, \tag{2.37}$$

respectively, where $\hat{\xi}=4\nu x/U_e a^2$.

Now we apply the method to solve the equations for V_1 and U_2. Putting $z=0$ in Eq. (2.31) and in an equation deduced from that equation by differentiating with respect to z, we obtain

$$\left.\begin{aligned} [\partial_{zz}V_1+\partial_z V_1/a-V_1/a^2]_{z=0}&=0, \\ [\partial_{zzz}V_1+\partial_{zz}V_1/a-2\partial_z V_1/a^2+2V_1/a^3]_{z=0}&=0. \end{aligned}\right\} \tag{2.38}$$

Equation (2.38) and the necessary wall condition fulfilled by V_1 suggest that as $z\to 0$,

$$V_1=U_e(1+\zeta)+B\{\zeta-\zeta^2/2+\zeta^3/2+O(\zeta^4)\}, \tag{2.39}$$

where B depends on x. Equation (2.39) can also be written

$$V_1=U_e((1+\zeta)+B\{\zeta(2+\zeta)/2(1+\zeta)+O(\zeta^4)\}. \tag{2.40}$$

It could be inferred that Eq. (2.40) is accurate near the wall, but an increase in $\hat{\xi}$ $(=4\nu x/U_e a^2)$ should decrease the role of the inertia terms, then V_1 becomes closer to the form which deletes the term $O(\zeta^4)$ in Eq. (2.40). Therefore we put

$$V_1=\begin{cases} U_e(1+\zeta)+U_e\beta_1^{-1}\zeta(2+\zeta)/2(1+\zeta)\ ;\ [\zeta\leqq\zeta_1=(1+2\beta_1)^{-1/2}-1], \\ 0 \qquad\qquad\qquad\qquad\qquad\qquad\ ;\ (\zeta\geqq\zeta_1), \end{cases} \tag{2.41}$$

where β_1 is an unknown parameter. The non-dimensional boundary layer thickness $\zeta_1=\delta_{y1}/a$ appearing in Eq. (2.41) is measured by the condition,

$$\delta_{y1}=[z]_{V_1=0}.$$

The wall shear stress composed in the peripheral direction is

$$\tau_{y1}=\mu[\partial_z V_1-V_1/(a+z)]_{z=0}=\mu U_e/a\beta_1. \tag{2.42}$$

Integration of Eq. (2.31) yields

$$\frac{d}{dx}\left\{\int_0^{\delta_{y1}} U_0 V_1(a+z)^2 dz\right\}=-\frac{a^2\tau_{y1}}{\rho}. \tag{2.43}$$

Introducing Eqs. (2.34), (2.41) and (2.42) into Eq. (2.43), we obtain

$$d\beta_1/d\xi=\beta_1\{\alpha_0 f_1(\beta_1)-\alpha_0^{-1}f_2(\beta_1)d\alpha_0/d\xi\}\ ;\ (\delta_{x0}\geqq\delta_{y1}), \tag{2.44}$$

$$\left.\begin{aligned} d\beta_1/d\xi&=\beta_1[\{(1+2\beta_1)h_1(\alpha_0)-h_2(\alpha_0)\}d\alpha_0/d\xi-8]/\{h_3(\alpha_0)+f_5(\beta_1)\}\ ; \\ &(\delta_{x0}\leqq\delta_{y1}). \end{aligned}\right\} \tag{2.45}$$

Functions $f_n(\beta_1)$ and $h_n(\alpha_0)$ are presented in Appendix 2. 1.

Turning now to the equations for U_2, the pressure gradient term $-\partial_x P_2/\rho$ in the second equation of Eq. (2.32) is expressed from the third equation as follows:

$$-\frac{\partial_x P_2}{\rho}=\partial_x\left\{\int_z^{\infty} V_1^2(a+z')^{-1}dz'\right\}=\int_1^{\delta_{y1}}\partial_x\{V_1^2(a+z')^{-1}\}dz'. \tag{2.46}$$

Putting $z=0$ in the second equation of Eq. (2.32) and in an equation derived by differentiation of that equation with respect to z, we obtain

$$[\partial_{zz}U_2+\partial_z U_2/a]_{z=0}=-\frac{1}{\nu}\int_0^{\delta_{y1}}\partial_x\{V_1^2(a+z')^{-1}\}dz', \tag{2.47 a}$$

$$[\partial_{zzz}U_2+\partial_{zz}U_2/a-\partial_z U_2/a^2]_{z=0}=0. \tag{2.47 b}$$

U_2 satisfying Eq. (2.47) behaves as

$$U_2=A\{\zeta-\zeta^2/2+\zeta^3/3+O(\zeta^4)\}+C\{2\zeta^2-2\zeta^3/3+O(\zeta^4)\}, \tag{2.48}$$

as $z\to 0$, where A depends on ξ, and C represents a contribution of the right-hand side of Eq. (2.47a) as follows:

$$C=-U_e\int_0^{\zeta_1}\partial_\xi\{(V_1/U_e)^2(1+\zeta)^{-1}\}d\zeta. \tag{2.49}$$

Equation (2.48) can be rewritten

$$U_2=A\{\ln(1+\zeta)+O(\zeta^4)\}+C\{\zeta(2+\zeta)-2\ln(1+\zeta)+O(\zeta^4)\}. \tag{2.50}$$

From Eq. (2.50) we can assume a suitable profile of U_2 as follows:

$$U_2=\left\{\begin{aligned} &U_e\alpha_2^{-1}\ln(1+\zeta) \\ &\quad+U_e f_3(\beta_1)(d\beta_1/d\xi)\{\zeta(2+\zeta)-2\ln(1+\zeta)\}/4\ ;\ (\zeta\leqq\zeta_2), \\ &0\qquad\qquad\qquad\qquad\qquad\qquad\qquad\qquad\ ;\ (\zeta\geqq\zeta_2), \end{aligned}\right\} \tag{2.51}$$

where α_2 is an unknown parameter and $f_3(\beta_1)$ is given in Appendix 2. 1. Also U_2

introduce a boundary layer thickness δ_{x2},

$$\delta_{x2}=[z]_{U_2=0}.$$

ζ_2 in Eq. (2.51) is non-dimensional boundary layer thickness δ_{x2}/a and it has a following relationship with α_2:

$$\alpha_2^{-1}=f_3(\beta_1)g_1(\zeta_2)d\beta_1/d\xi. \tag{2.52}$$

The contribution of U_2 to the wall shear stress is written

$$\tau_{x2}=\mu[\partial_z U_2]_{z=0}=\mu U_e/a\alpha_2. \tag{2.53}$$

The momentum integral equation for U_2 is

$$\frac{d}{dx}\left\{\int_0^{\delta_{x2}}U_2(U_e-2U_0)(a+z)dz+\int_0^{\delta_{y1}}(a+z)\int_z^{\delta_{y1}}\frac{V_1^2}{a+z'}dz'dz\right\}=\frac{a\tau_{x2}}{\rho}. \tag{2.54}$$

Instead of the equation of α_2 we consider an equation of ζ_2 obtained by introducing Eqs. (2.34), (2.41), (2.51), (2.52) and (2.53) into Eq. (2.54). We should consider whether δ_{x0} is greater than δ_{x2} or not, because Eq. (2.54) contains U_0. Since the calculated results showed that always the relation $\delta_{x0}\geqq\delta_{x2}$ was satisfied, only the equation for that case is shown as follows:

$$\left.\begin{aligned}d\zeta_2/d\xi=[&\alpha_0\{g_1(\zeta_2)-f_4(\beta_1)\}+\alpha_0^{-1}g_4(\zeta_2)d\alpha_0/d\xi\\&-\{(d^2\beta_1/d\xi^2)(d\beta_1/d\xi)^{-1}-4\beta_1^{-1}f_4(\beta_1)d\beta_1/d\xi\}\{g_4(\zeta_2)\\&+\alpha_0 g_5(\zeta_2)\}]/\{g_2(\zeta_2)-\alpha_0 g_3(\zeta_2)\}g_6(\zeta_2),\end{aligned}\right\} \tag{2.55}$$

where $g_n(\zeta_2)$ and $d^2\beta_1/d\xi^2$ are presented in Appendix 2. 1.

2. 3. 3. A solution near the origin

The boundary layer thickness at the origin is zero, then

$$[\alpha_0]_{\xi=0}=[\beta_1]_{\xi=0}=[\zeta_2]_{\xi=0}=0. \tag{2.56}$$

Although the behavior of all Eqs. (2.36), (2.44, 45) and (2.55) appear as indefinite at the origin, $|\alpha_0|$, $|\beta_1|$ and $|\zeta_2|\ll 1$ near the origin then an expansion of Eq. (2.36) becomes

$$d\alpha_0/d\xi=3\alpha_0^{-1}(1-2\alpha_0+\cdots)/2. \tag{2.57}$$

It has a solution

$$\alpha_0=\sqrt{3\xi}(1-2\sqrt{3\xi}/3+\cdots). \tag{2.58}$$

Using undetermined multiplier A_n, we put β_1 as

$$\beta_1=A_1\alpha_0+A_2\alpha_0^2+\cdots. \tag{2.59}$$

Considering Eq. (2.57), from Eq. (2.59) we obtain

$$d\beta_1/d\xi=3\alpha_0^{-1}\{A_1-2(A_1-A_2)\alpha_0+\cdots\}/2. \tag{2.60}$$

Expansions of Eqs. (2.44, 45) are

$$\left.\begin{aligned} d\beta_1/d\xi=3\alpha_0^{-1}\{&(A_1^3-1)A_1^{-2}/2+(7A_1^2/8-A_1-21A_1^{-1}/8\\ &+A_1^{-3}A_2+A_2/2)\alpha_0+\cdots\}/2\,;\ (\delta_{x0}\geqq\delta_{y1}), \end{aligned}\right\} \tag{2.61}$$

$$\left.\begin{aligned} d\beta_1/d\xi=3\alpha_0^{-1}[&A_1(1+3A_1)(1-3A_1^2)^{-1}+A_1(1-3A_1^2)^{-1}\{1+4A_1\\ &+2A_1^{-1}A_2+12A_2-3(1+3A_1)(1-3A_1^2)^{-1}(1+8A_1^3\\ &-4A_1A_2)\}\alpha_0/2+\cdots]/2\,;\ (\delta_{x0}\leqq\delta_{y1}). \end{aligned}\right\} \tag{2.62}$$

Comparisons between Eqs. (2.61, 62) and Eq. (2.60) show that $A_1=-1$ and $A_2=1$ irrespective $\delta_{x0}\geqq\delta_{y1}$ or $\delta_{x0}\leqq\delta_{y1}$, then we obtain

$$\beta_1=-\alpha_0+\alpha_0^2+\cdots. \tag{2.63}$$

Substitution of Eq. (2.58) into Eq. (2.63) yields

$$\beta_1=-\sqrt{3\xi}(1-5\sqrt{3\xi}/3+\cdots). \tag{2.64}$$

Similar method applied to ζ_2 gives a following expression:

$$\zeta_2=\sqrt{3\xi}(1-23\sqrt{3\xi}/60+\cdots). \tag{2.65}$$

Whence follows

$$\alpha_2=1+31\sqrt{3\xi}/20+\cdots. \tag{2.66}$$

Now we will examine the boundary layer thicknesses δ_{x0}, δ_{y1} and δ_{x2} near the origin. δ_{x0} can be expressed by use of Eq. (2.34) and Eq. (2.58) as follows:

$$\delta_{x0}=a(\alpha_0+\alpha_0^2/2+\cdots)=a\sqrt{3\xi}(1-\sqrt{3\xi}/6+\cdots). \tag{2.67}$$

δ_{y1} is obtained from Eq. (2.41) as

$$\delta_{y1}=a(-\beta_1+3\beta_1^2/2+\cdots)=a\sqrt{3\xi}(1-\sqrt{3\xi}/6+\cdots). \tag{2.68}$$

δ_{x2} is

$$\delta_{x2}=a\sqrt{3\xi}(1-23\sqrt{3\xi}/60+\cdots). \tag{2.69}$$

Expansions of δ_{x0} and δ_{y1} coincide at least to the second order term, then it may be inferred that near the leading edge two boundary layer thicknesses have the same value. Also the condition of $\delta_{x0}\geqq\delta_{x2}$ on which Eq. (2.55) is based is satisfied near the origin.

2. 3. 4. Numerical procedure

The problem reduces to the numerical calculation of Eqs. (2.36), (2.44, 45) and (2.55), but to obtain the result was found rather subtle and difficult because they have a form 0/0 at the origin. We should seek some tricks. Eqs. (2.36), (2.44, 45) and (2.55) were transformed into the forms which contain α_0^2, β_1^2 and ζ_2^2 instead of α_0, β_1 and ζ_2 respectively. Still they behave as 0/0 at the origin, but we can infer the limits by use of Eqs. (2.58), (2.64) and (2.65) as follows:

$$[d\alpha_0^2/d\xi]_{\xi=0}=[d\beta_1^2/d\xi]_{\xi=0}=[d\zeta_2^2/d\xi]_{\xi=0}=3. \tag{2.70}$$

Near the origin we use the equations whose right-hand sides have expanded terms respectively with assumptions, $|\alpha_0|$, $|\beta_1|$ and $|\zeta_2|\ll 1$. Number of those terms which should be contained in the expansions was determined to assure 8 significant figures at the point where calculation of equations having expanded terms was changed to the calculation of the original ones. From Eq. (2.36) we obtain an expanded equation for α_0^2,

$$d\alpha_0^2/d\xi=3/(1+2\alpha_0+9\alpha_0^2/5+16\alpha_0^3/15). \tag{2.71}$$

The other equations for β_1^2 and ζ_2^2 are formaly same to the equations which are obtained by the multiplication of $2\beta_1$ and $2\zeta_2$ to Eqs. (2.44, 45) and (2.55) respectively, but functions $f_n(\beta_1)$, $g_n(\zeta_2)$ and $h_n(\alpha_0)$, and $d^2\beta_1/d\xi^2$ contained in those equations are expanded; they are shown in Appendix 2. 2.

As a first step expanded equations were solved using initial values: Eqs. (2.56) and (2.70), and then at the suitable point computation of the original equations were started to match the value obtained by the expanded equations. Numerical method used was Hamming's method and double precision arithmetic was employed.

2. 3. 5. Results and discussion

Comparisons of two terms series solution near the origin using undetermined multipliers, Eqs. (2.58), (2.64), (2.65) and (2.66), with numerical results are shown in Fig. 2. 10. Agreement is excellent near the origin. In the present calculation range $0\leqq\xi\leqq 10^4$, δ_{y1} was greater than or equal to δ_{x0}, and the condition $\delta_{x0}\geqq\delta_{x2}$ was always satisfied.

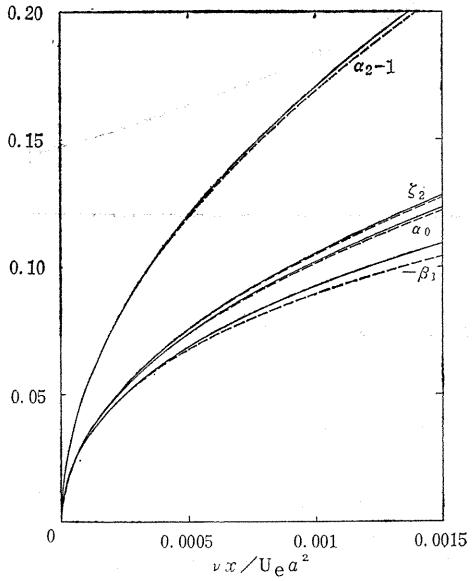

Fig. 2. 10. Behavior of various parameters near the origin; solid line represents the numerical results, and dotted line shows the series solution near the origin.

Wall shear stress components are expressed in non-dimensional form as follows:

$$\left.\begin{aligned} a\tau_x/\mu U_e &= aU_e^{-1}[\partial_z U]_{z=0} = \alpha_0^{-1} + \Omega^2\alpha_2^{-1} + \cdots, \\ a\tau_y/\mu V_w &= aV_w^{-1}[\partial_z V - V/(a+z)]_{z=0} = \beta_1^{-1} + \cdots. \end{aligned}\right\} \tag{2.72}$$

Calculated results are shown in Fig. 2. 11 as non-dimensional frictional forces acting on the unit length of a cylinder. The effect of Ω on $a\tau_x/\mu U_e$ appears within a limited range of $\nu x/U_e a^2$. This fact can be explained by the equation obtained from Eqs. (2.58) and (2.66), that is,

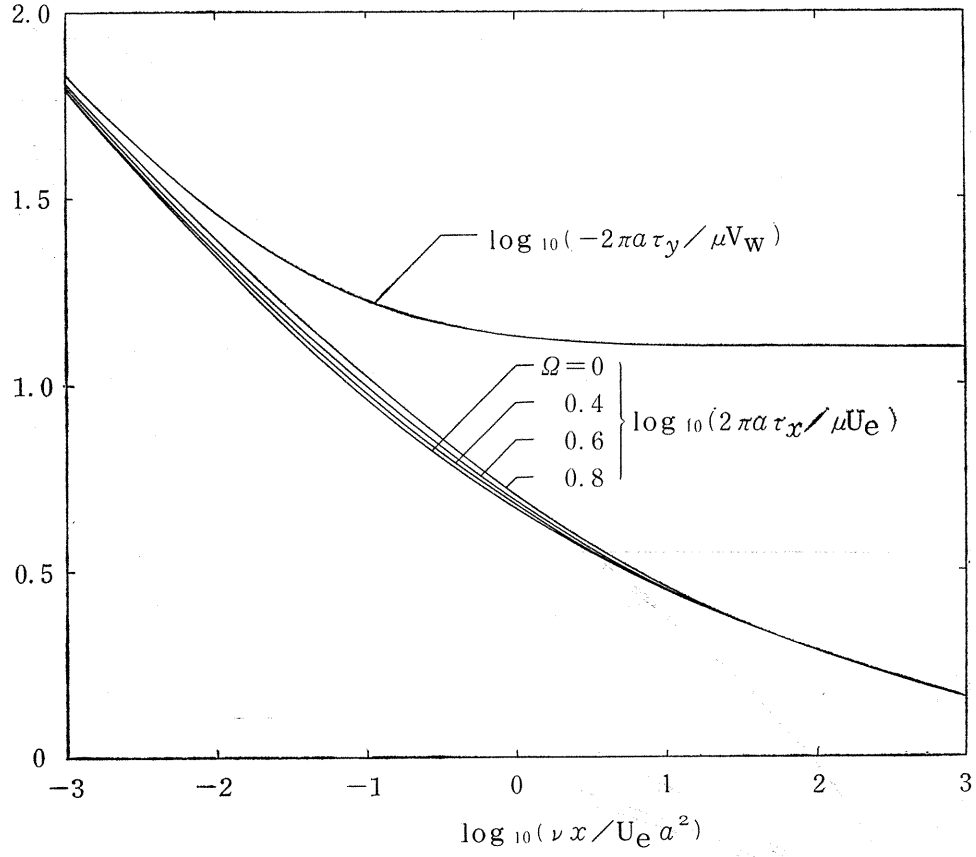

Fig. 2. 11. Non-dimensional wall shear-force components per unit length of the cylinder.

$$a\tau_x/\mu U_e = \alpha_0^{-1}\{1 + \Omega^2\sqrt{3\xi}(1 - 133\sqrt{3\xi}/60 + \cdots) + \cdots\}. \tag{2.73}$$

Then we can infer that the effect of Ω reduces with $\xi \to 0$. As $\xi \to \infty$, on the other hand, the variation of peripheral velocity distribution with x reduces, then the effect of Ω on the wall shear stress also decreases.

In the same figure, non-dimensional wall shear force in the y-direction is presented and it represents the result of zeroth order with respect to Ω. It coincides with the value of x-direction near the origin. This behavior reflects the fact that $\beta_1 \to -\alpha_0$ when $\xi \to 0$, and physically it shows that the boundary layer thickness

is thin with respect to the cylinder radius. Sufficiently far from the leading edge the inertia effect becomes less significant, then the problem reduces to a rotating cylinder in an quiescent fluid. In such a case we can solve the Navier-stokes equation exactly and obtain the value 2 of $-a\tau_y/\mu V_w$. In Fig. 2. 11 the trend $-a\tau_y/\mu V_w \to 2$ as $\nu x/U_e a^2 \to \infty$ is evident.

Displacement thickness Δ_x and momentum thickness Θ_x of a thin cylinder have the following non-dimensional expressions:

$$\left.\begin{aligned}
\frac{\Delta_x}{a} &= \int_0^{\infty}\left(1-\frac{U}{U_e}\right)(1+\zeta)d\zeta \\
&= \int_0^{\zeta_0}\left(1-\frac{U_0}{U_e}\right)(1+\zeta)d\zeta - \Omega^2\int_0^{\zeta_2}\frac{U_2}{U_e}(1+\zeta)d\zeta+\cdots, \\
\frac{\Theta_x}{a} &= \int_0^{\infty}\frac{U}{U_e}\left(1-\frac{U}{U_e}\right)(1+\zeta)d\zeta \\
&= \int_0^{\zeta_0}\frac{U_0}{U_e}\left(1-\frac{U_0}{U_e}\right)(1+\zeta)d\zeta + \Omega^2\int_0^{\zeta_2}\frac{U_2}{U_e}\left(1-2\frac{U_0}{U_e}\right)(1+\zeta)d\zeta+\cdots.
\end{aligned}\right\} \quad (2.74)$$

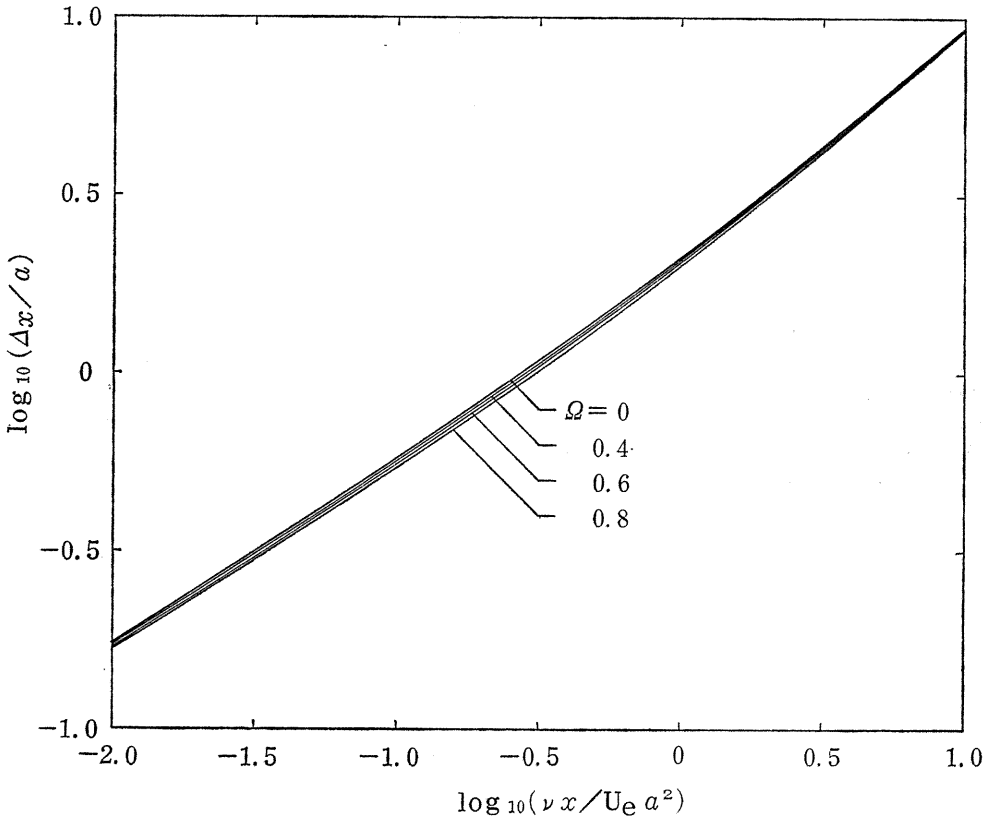

Fig. 2. 12. Non-dimensional displacement thickness.

Calculated results of Δ_x/a are shown in Fig. 2. 12. The effect of Ω is rather small. Table 2. 3 gives the value of $\log_{10}(\Theta_x/a)$. Angular momentum thickness

Table 2. 3. Variation of $\log_{10}(\theta_x/a)$ with the speed ratio Ω.

$\frac{\nu x}{U_e a^2}$	Ω			
	0	0.4	0.6	0.8
10^{-3}	−1.723	−1.723	−1.723	−1.724
10^{-2}	−1.194	−1.194	−1.194	−1.195
10^{-1}	−0.621	−0.622	−0.623	−0.625
1	0.027	0.025	0.023	0.019
10	0.759	0.758	0.757	0.755
10^2	1.565	1.564	1.564	1.563
10^3	2.420	2.420	2.420	2.420

Θ_{xy} and a parameter Θ_{yy} which represents the pressure variation due to the rotation are written

$$\left.\begin{aligned}\frac{\theta_{xy}}{a}&=\int_0^\infty \frac{U}{U_e}\frac{V}{V_w}(1+\zeta)^2 d\zeta\\&=\int_0^{\zeta_1}\frac{U_0}{U_e}\frac{V_1}{U_e}(1+\zeta)^2 d\zeta+\cdots,\\\frac{\theta_{yy}}{a}&=\int_0^\infty(1+\zeta)\int_\zeta^\infty\left(\frac{V}{V_w}\right)^2\frac{1}{1+\zeta'}d\zeta' d\zeta\\&=\int_0^{\zeta_1}(1+\zeta)\int_\zeta^{\zeta_1}\left(\frac{V_1}{U_e}\right)^2\frac{1}{1+\zeta'}d\zeta' d\zeta+\cdots.\end{aligned}\right\}\qquad(2.75)$$

Calculated results of Θ_{xy}/a and Θ_{yy}/a are shown in Fig. 2. 13. Above mentioned effect of Ω on various quantities of the boundary layer comes from the acceleration produced by the pressure change due to the rotation. $-\Theta_{yy}$ estimated from Fig. 2. 13 represents an equivalent parameter of external pressure appearing in the momentum integral equation.

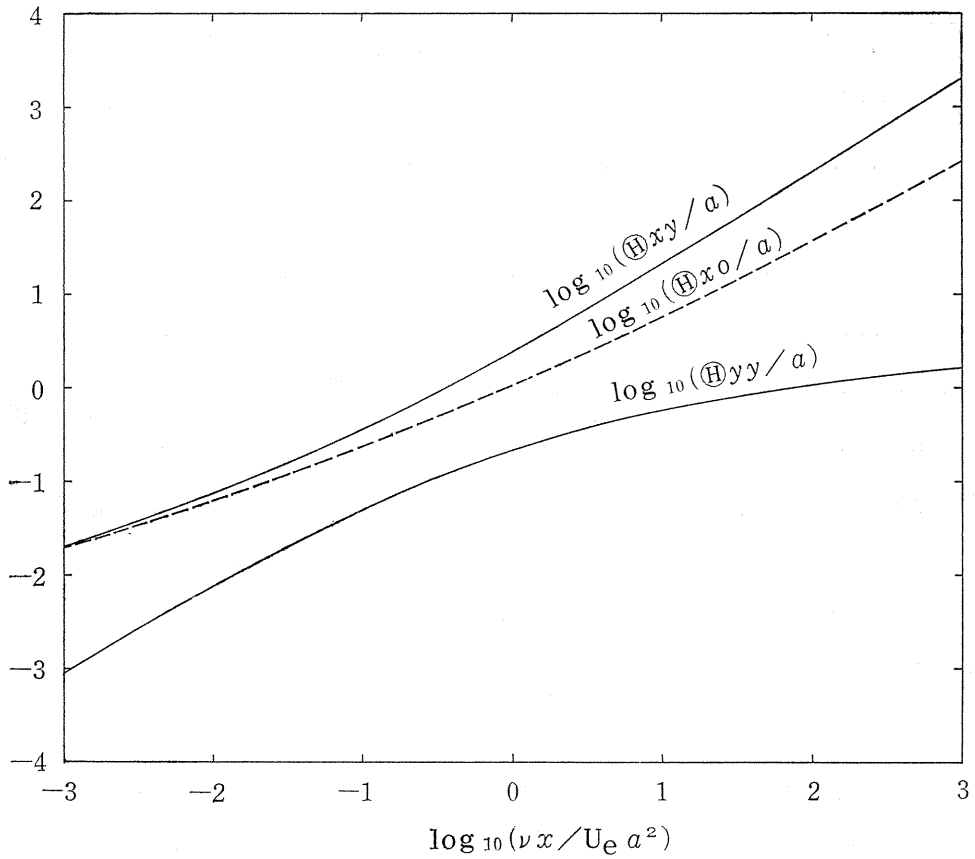

Fig. 2. 13. Non-dimensional momentum thickness θ_{xy} and parameter θ_{yy}. θ_{x0} represents the value of θ_x at $\Omega=0$.

Appendix 2. 1. Defining equations for $f_n(\beta_1)$, $g_n(\zeta_2)$ and $h_n(\alpha_0)$, and second order derivatives of β_1 with respect to ξ.

$$
\left.
\begin{aligned}
f_1(\beta_1) &= 4(1+2\beta_1)^2/\{(1+4\beta_1)\ln(1+2\beta_1)-2\beta_1(1+3\beta_1)\},\\
f_2(\beta_1) &= (1+2\beta_1)\{\ln(1+2\beta_1)-2\beta_1(1-\beta_1)\}\\
&\quad /\{(1+4\beta_1)\ln(1+2\beta_1)-2\beta_1(1+3\beta_1)\},\\
f_3(\beta_1) &= 2\beta_1^{-3}\{(1+\beta_1)\ln(1+2\beta_1)-2\beta_1\},\\
f_4(\beta_1) &= \{(3+8\beta_1+4\beta_1^2)\ln(1+2\beta_1)-2\beta_1(3+5\beta_1)\}\\
&\quad /[4(1+2\beta_1)\{(1+\beta_1)\ln(1+2\beta_1)-2\beta_1\}],\\
f_5(\beta_1) &= 4(1+4\beta_1)/(1+2\beta_1)^2.
\end{aligned}
\right\} \qquad (2.76)
$$

$$\left.\begin{aligned}
g_1(\zeta_2)&=\{2\ln(1+\zeta_2)-\zeta_2(2+\zeta_2)\}/4\ln(1+\zeta_2),\\
g_2(\zeta_2)&=[(1+\zeta_2)^2\{2\ln^2(1+\zeta_2)-2\ln(1+\zeta_2)+1\}-1]/2,\\
g_3(\zeta_2)&=[(1+\zeta_2)^2\{2\ln(1+\zeta_2)-1\}+1]/4,\\
g_4(\zeta_2)&=\zeta_2(2+\zeta_2)g_2(\zeta_2)/\ln(1+\zeta_2)+2g_3(\zeta_2)\\
&\quad-[(1+\zeta_2)^4\{4\ln(1+\zeta_2)-1\}+1]/8,\\
g_5(\zeta_2)&=\zeta_2(2+\zeta_2)\{\zeta_2(2+\zeta_2)/4-g_3(\zeta_2)/\ln(1+\zeta_2)\},\\
g_6(\zeta_2)&=\{2(1+\zeta_2)^2\ln(1+\zeta_2)-\zeta_2(2+\zeta_2)\}/(1+\zeta_2)\ln^2(1+\zeta_2).
\end{aligned}\right\}\tag{2.77}$$

$$\left.\begin{aligned}
&h_1(\alpha_0)=\alpha_0^{-2}\{1-(1-4\alpha_0)e^{4\alpha_0}\},\quad h_2(\alpha_0)=4\alpha_0^{-2}\{1-(1-2\alpha_0)e^{2\alpha_0}\},\\
&h_3(\alpha_0)=\alpha_0^{-1}(3-4e^{2\alpha_0}+e^{4\alpha_0}),\quad h_4(\alpha_0)=(2-3\alpha_0+2\alpha_0^2)e^{2\alpha_0}-(2+\alpha_0).
\end{aligned}\right\}\tag{2.78}$$

$$\left.\begin{aligned}
d^2\beta_1/d\xi^2&=\beta_1^{-1}(d\beta_1/d\xi)^2+\beta_1[\alpha_0^{-2}f_2(\beta_1)(d\alpha_0/d\xi)^2-\alpha_0^{-1}f_2'(\beta_1)(d\alpha_0/d\xi)(d\beta_1/d\xi)\\
&\quad+[f_1(\beta_1)+f_2(\beta_1)h_4^{-2}(\alpha_0)\{\alpha_0h_4'(\alpha_0)-2h_4(\alpha_0)\}]d\alpha_0/d\xi\\
&\quad+\alpha_0f_1'(\beta_1)d\beta_1/d\xi];\ (\delta_{x0}\geqq\delta_{y1}),\\
d^2\beta_1/d\xi^2&=\beta_1^{-1}(d\beta_1/d\xi)^2+\beta_1[[\{(1+2\beta_1)h_1'(\alpha_0)-h_2'(\alpha_0)\}\{h_3(\alpha_0)+f_5(\beta_1)\}\\
&\quad-\{(1+2\beta_1)h_1(\alpha_0)-h_2(\alpha_0)\}h_3'(\alpha_0)](d\alpha_0/d\xi)^2+[2h_1(\alpha_0)\\
&\quad\times\{h_3(\alpha_0)+f_5(\beta_1)\}-\{(1+2\beta_1)h_1(\alpha_0)-h_2(\alpha_0)\}f_5'(\beta_1)](d\alpha_0/d\xi)(d\beta_1\\
&\quad/d\xi)-[\{(1+2\beta_1)h_1(\alpha_0)-h_2(\alpha_0)\}\{h_3(\alpha_0)+f_5(\beta_1)\}\alpha_0h_4^{-2}(\alpha_0)\\
&\quad\times\{\alpha_0h_4'(\alpha_0)-2h_4(\alpha_0)\}-8h_3'(\alpha_0)]d\alpha_0/d\xi+8f_5'(\beta_1)d\beta_1/d\xi]\\
&\quad/\{h_3(\alpha_0)+f_5(\beta_1)\}^2;\ (\delta_{x0}\leqq\delta_{y1}),
\end{aligned}\right\}\tag{2.79}$$

where the prime denotes the differentiations with respect to the respective arguments.

Appendix 2. 2. Expanded expressions of $f_n(\beta_1)$, $g_n(\zeta_2)$, $h_n(\alpha_0)$, and their derivatives included in Eq. (2. 79).

$$\left.\begin{aligned}
f_1(\beta_1)&=-3\beta_1^{-3}(1+21\beta_1/4+701\beta_1^2/80)/4,\\
f_2(\beta_1)&=-(1+7\beta_1/4-17\beta_1^2/80)/2,\\
f_3(\beta_1)&=4(1-2\beta_1+18\beta_1^2/5)/3,\\
f_4(\beta_1)&=\beta_1(1-8\beta_1/5+14\beta_1^2/5-892\beta_1^3/175)/2,\\
f_5(\beta_1)&=4(1-4\beta_1^2+16\beta_1^3-48\beta_1^4).
\end{aligned}\right\}\tag{2.80}$$

$$
\left.\begin{aligned}
g_1(\zeta_2)&=-\zeta_2(1+\zeta_2/6-\zeta_2^3/180)/2,\\
g_2(\zeta_2)&=2\zeta_2^3(1-\zeta_2^2/20+\zeta_2^3/24)/3,\\
g_3(\zeta_2)&=\zeta_2^2(1+\zeta_2/3-\zeta_2^2/12+\zeta_2^3/30)/2,\\
g_4(\zeta_2)&=\zeta_2^4(1+4\zeta_2/15-\zeta_2^2/30+\zeta_2^3/630)/3,\\
g_5(\zeta_2)&=-\zeta_2^3(1+\zeta_2/2+\zeta_2^2/60-\zeta_2^3/120)/3,\\
g_6(\zeta_2)&=2(1+\zeta_2/3+\zeta_2^3/180).
\end{aligned}\right\}\qquad(2.81)
$$

$$
\left.\begin{aligned}
h_1(\alpha_0)&=8(1+8\alpha_0/3+4\alpha_0^2+64\alpha_0^3/15),\\
h_2(\alpha_0)&=8(1+4\alpha_0/3+\alpha_0^2+8\alpha_0^3/15),\\
h_3(\alpha_0)&=-4(1-4\alpha_0^2/3-2\alpha_0^3-28\alpha_0^4/15),\\
h_4(\alpha_0)&=2\alpha_0^3(1+2\alpha_0+9\alpha_0^2/5+16\alpha_0^3/15)/3.
\end{aligned}\right\}\qquad(2.82)
$$

$$
\left.\begin{aligned}
f_1'(\beta_1)&=9\beta_1^{-4}(1+7\beta_1/2+701\beta_1^2/240)/4,\\
f_2'(\beta_1)&=-7(1-17\beta_1/70)/8,\\
f_5'(\beta_1)&=-32\beta_1(1-6\beta_1+24\beta_1^2).
\end{aligned}\right\}\qquad(2.83)
$$

$$
\left.\begin{aligned}
h_1'(\alpha_0)&=64(1+3\alpha_0+24\alpha_0^2/5)/3,\\
h_2'(\alpha_0)&=32(1+3\alpha_0/2+6\alpha_0^2/5)/3,\\
h_3'(\alpha_0)&=32\alpha_0(1+9\alpha_0/4+14\alpha_0^2/5)/3,\\
h_4'(\alpha_0)&=2\alpha_0^2(1+8\alpha_0/3+3\alpha_0^2).
\end{aligned}\right\}\qquad(2.84)
$$

Ⅲ Experiments on the Thick Turbulent Boundary Layers on Rotating Bodies with a Roughness Element

3. 1. Introduction

The turbulent boundary layers which develop on a spinning body of revolution have the same salient features as the laminar ones studied theoretically in Chapter Ⅱ; the effects of the rotation and the transverse curvature of the body dominate the behavior of these flows. Since the growth rate of the turbulent boundary layers are greater than that of the laminar ones, these effects appearing in connection with the radius of the body are more important in turbulent flows.

Moreover, the phenomena of turbulent flows are so complex that no general approach to the solution of the problems exists; it is still next to impossible to make accurate quantitative prediction without relying heavily on empirical data. The history of the developments of many researches on two-dimensional turbulent

boundary layers indicates that a lot of experiments under various conditions must also be made in order to resolve the present problems of these complicated turbulent flows.

Generally speaking, of many factors that determine the behavior of the turbulent boundary layers on a flat plate, two external conditions, i. e., the pressure gradient in the free stream and the surface roughness, are fundamental and decisive. In the present problem also it is apparently important to examine separately the effect of these two factors, and perhaps the knowledge obtained through these researches will serve for the practice in the design of fluid machinery.

This chapter deals with the effect of the roughness element; the experimental investigation is made of those relatively thick turbulent boundary layers developing on the spinning cylinder in a uniform flow which are strongly disturbed by a ring or a backward step. The disturbance introduced in the boundary layer promote the development of the layer so that the effect of curvature becomes significant. Another important role of the roughness element is to destroy the quasi-collateral condition which was confirmed experimentally in the previous ordinary cases[4] and used as a basis of the prediction[3].

Descriptions are made firstly of the preliminary consideration on the curvature effect. Next, measurements of velocity distribution in the skewed turbulent boundary layers affected by the roughness element are presented and discussed in detail. Thirdly, the condition of the quasi-collateral relationship is extended to the thick boundary layer and compared with the measured velocity profiles. In this connection, a shape parameter which may describe quantitatively the deviation of the velocity profiles from that condition will be discussed.

3. 2. Basic consideration

The effect of curvature on the boundary layer may be clarified by use of the equation of motion. Writing down the equation of mean motion in the cylindrical coordinate and estimating the order of magnitude of each terms following to Hinze [45] then gives the following equations taking the second order terms;

$$\left.\begin{aligned} &\partial_x(rU)+\partial_r(rW)=0,\\ &U\partial_xU+W\partial_rU=-\partial_xP/\rho+\partial_r(r\tau_x)/\rho r,\\ &U\partial_xV+W\partial_rV+VW/r=\partial_r(r^2\tau_y)/\rho r^2,\\ &V^2/r=\partial_rP/\rho+(\overline{w}^2-\overline{v}^2)/r+\partial_r\overline{w}^2, \end{aligned}\right\} \tag{3.1}$$

and boundary conditions are

$$\left.\begin{aligned} &r=a\ :\ U=W=u=v=w=0,\quad V=V_0=a\omega,\\ &r\to\infty\ :\ U\to U_e,\quad V,\ u,\ v,\ w\to 0, \end{aligned}\right\} \tag{3.2}$$

where τ_x and τ_y are shearing stress components represented as follows:

$$\left.\begin{aligned} &\tau_x=\mu\partial_rU-\rho\overline{uw},\\ &\tau_y=\mu(\partial_rV-V/r)-\rho\overline{vw}. \end{aligned}\right\} \tag{3.3}$$

It may be plausible to express the effect of curvature by use of momentum thicknesses. Then we derive the mometum integral equations:

$$\left.\begin{aligned}&\frac{d}{dx}\{\rho U_e^2(\Theta_x+\theta_r'-\theta_{rr}')\}-\Delta_x\frac{dP_e}{dx}+\frac{d}{dx}\{\rho V_0^2(\Theta_{yy}+\theta_{yy}')\}=\tau_{0x},\\&\frac{d}{dx}(\rho U_e V_0\Theta_{xy})=-\tau_{0y},\end{aligned}\right\}\qquad(3.4)$$

where τ_{0x} and τ_{0y} are the components of wall shear stress. Various thicknesses appearing in above equations are defined by the integrals:

$$\left.\begin{aligned}&\Theta_x=\int_a^{r_\delta}\frac{U}{U_e}\left(1-\frac{U}{U_e}\right)\frac{r}{a}dr,\quad \Delta_x=\int_a^{r_\delta}\left(1-\frac{U}{U_e}\right)\frac{r}{a}dr,\\&\Theta_{xy}=\int_a^{r_\delta}\frac{U}{U_e}\frac{V}{V_0}\left(\frac{r}{a}\right)^2dr,\quad \Theta_{yy}=\int_a^{r_\delta}\frac{r}{a}\int_r^{r_\delta}\left(\frac{V}{V_0}\right)^2\frac{1}{r'}dr'dr,\end{aligned}\right\}\qquad(3.5\,a)$$

and

$$\left.\begin{aligned}&\theta_r'=\int_a^{r_\delta}\frac{\overline{w^2}}{U_e^2}\frac{r}{a}dr,\quad \theta_{rr}'=\int_a^{r_\delta}\frac{r}{a}\int_r^{r_\delta}\frac{\overline{w^2}}{U_e^2}\frac{1}{r'}dr'dr,\\&\theta_{yy}'=\int_a^{r_\delta}\frac{r}{a}\int_r^{r_\delta}\frac{\overline{v^2}}{V_0^2}\frac{1}{r'}dr'dr.\end{aligned}\right\}\qquad(3.5\,b)$$

The thickness Θ_{yy} is an integral of the static pressure variation due to the rotation, and the thicknesses as θ_r', θ_{rr}' and θ_{yy}' introduced here, which express the contributions of Reynolds normal stresses, make the equation to a simple form. Since Hinze's estimation suppresses the term $\partial_x\overline{u^2}$ the corresponding thickness does not appear. As Moore's consideration[46] in the case of stationary cylinder, we can compare the boundary layer with potential flow using the thicknesses θ_{xa} and δ_{xa}^* defined by Θ_x and Δ_x, that is,

$$\left.\begin{aligned}&\{(a+\theta_{xa})^2-a^2\}/2a=\Theta_x,\\&\{(a+\delta_{xa}^*)^2-a^2\}/2a=\Delta_x.\end{aligned}\right\}\qquad(3.6\,a)$$

Inviscid flow rotating as rigid body may serve as a thickness which plays a role for Θ_{xy} as a reference as do the θ_{xa} and δ_{xa}^* for Θ_x and Δ_x. Then a thickness θ_{xya} can be defined by

$$\int_a^{a+\theta_{xya}}\left(\frac{r}{a}\right)^3dr=\Theta_{xy}.\qquad(3.6\,b)$$

The thicknesses δ_x^*, θ_x and θ_{xy} used so far mainly by authors are reduced when $a\to\infty$ with fixed z $(=r-a)$ in the definition of Δ_x, Θ_x and Θ_{xy} respectively, so it can be seen by comparing these thicknesses whether or not the effect of curvature must be taken to account. Some values of these parameters evaluated from the measured velocity distribution are presented in Table 3. 1. It may be concluded that Θ_x and Θ_{xy} must be considered instead of θ_x and θ_{xy} respectively when the boundary layer thickness grows about 20% of the cylinder radius. As the

square of the distance from the cylinder axis appears in the defining equation of Θ_{xy}, the curvature affects this thickness more than Θ_x, so the curvature effect appears in earlier stage of boundary layer development in the case of rotating cylinder than with stationary cylinder.

Table 3. 1. The thicknesses of the boundary layer in the case of Cylinder.

$\bar{x}$=510mm				$\bar{x}$=657mm			
Ω_m	δ/a	θ_x/θ_x	θ_{xy}/θ_{xy}	Ω_m	δ/a	θ_x/θ_x	θ_{xy}/θ_{xy}
1	0.22	1.07	1.15	1	0.34	1.10	1.19
2	0.37	1.11	1.23	2	0.45	1.14	1.31

3. 3. Experimental apparatus and procedures

The tunnel employed is suction type with a circular working section of 350 mm diameter. The details are described in Ref. 4). Experiments were carried out using four shapes of rotating bodies as shown in Fig. 3. 1. They are as follows: Ⅰ) cylinder with no roughness, Ⅱ) cylinder with a ring of 2.5 mm height and 2.5 mm breadth, Ⅲ) cylinder with a ring of 5 mm height and 2.5 mm breadth, and Ⅳ) cylinder with a backward facing step of 5 mm height. In what follows these are designated as Ⅰ) Cylinder, Ⅱ) Ring 2.5, Ⅲ) Ring 5, and Ⅳ) Step, respectively.

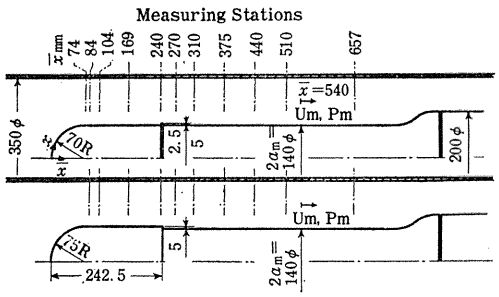

Fig. 3. 1. Experimental arrangements and measuring stations.

In order to generate disturbance in the turbulent boundary layer, rings and a step were placed at the station where the values of Reynolds number based on the momentum thickness of the stationary cylinder were greater than the critical value which is a criterion of fully developed turbulent boundary layer given by Preston[47]. The measured value of $R_{\theta x}$ at $\bar{x}$=240 mm was 530 and the total thickness of the layer was about 8 mm at that position. Then the height of rings and a step was determined to ensure that these elements immersed enough in the layer.

A three-hole yaw probe with a flattened tip of 0.5 mm height was used to measure the velocity distribution and a static probe also used, orienting to the flow direction which was determined by the yaw probe. The directional sensitivity of the yaw probe and the detailed description of measuring method are presented in Ref. 4).

The value of Reylolds number based on the reference velocity and the radius of the body as shown in Fig. 3. 1 was fixed at 5×10^4 throughout the experiments and speed ratio $\Omega_m(=a_m\omega/U_m)$ was varied from zero to 1 and 2.

3. 4. Measured velocity profiles

3. 4. 1. The case of Cylinder

In the first place we will describe the results of measurements carried out with a cylinder which provide a reference as a standard case for the other rotating bodies.

Pressure distribution on the wall of the duct and at various heights from the cylinder surface measured at $\Omega_m=0$ is presented in Fig. 3. 2. This figure shows

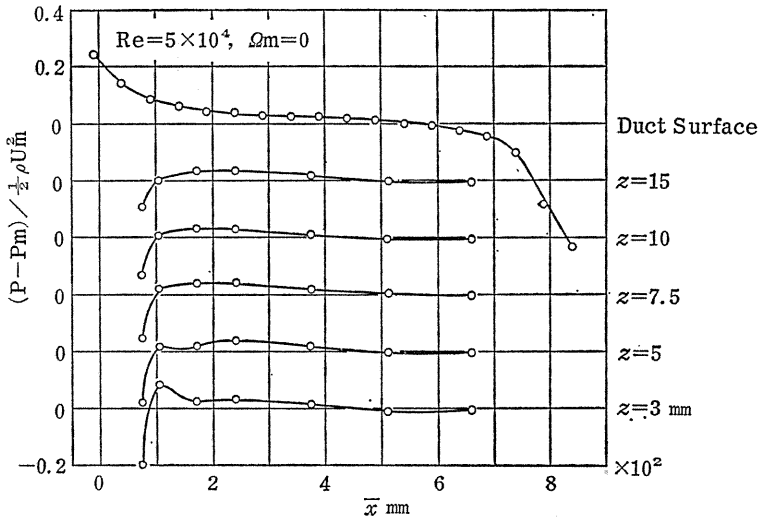

Fig. 3. 2. Pressure distribution in the case of Cylinder.

that the static pressure is effectively constant between the stations of $\bar{x}=169$ mm and 657 mm.

Velocity profiles on the stationary cylinder are shown in Fig. 3. 3 using non-dimensional velocity and distance from the cylinder surface specified by free stream velocity outside of the layer U_e and the momentum thickness θ_x defined in Eq. (3. 5 a), respectively. In the range of these experiments this figure clearly shows similar velocity profiles of turbulent boundary layer.

The components of velocity in the axial direction and in the peripheral direction are presented in Fig. 3. 4. The velocity scale in the peripheral direction is naturally surface velocity V_0, and the distance from the cylinder surface is divided by θ_{xy} instead of θ_x since it was found that in the rotating case the non-dimensional distance z/θ_{xy} shows more similarity in the velocity profiles in both directions than does z/θ_x when comparing the axial velocity distribution with Fig. 3. 3. The profiles are not so similar as seen with a stationary cylinder even in the same range of $\bar{x}$. Obviously rotation fosters the development of the boundary layers in

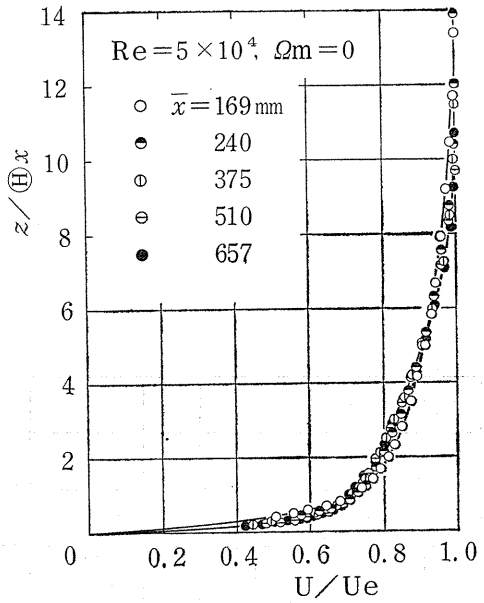

Fig. 3. 3. Velocity profiles in the turbulent boundary layer for Cylinder at $\Omega_m=0$.

such a way that they lose similarity in the form of U/U_e vs. z/Θ_x or z/Θ_{xy} within the same range of axial distance as in the stationary case.

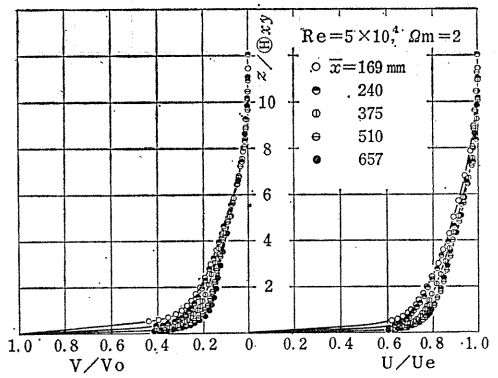

Fig. 3. 4. Velocity profiles for Cylinder at $\Omega_m=2$.

3. 4. 2. The cases of Ring 2.5 and of Ring 5

Pressure distributions for Ring 2.5 and Ring 5 are presented in Figs. 3. 5 and 3. 6, respectively. At the section of the ring, the pressure decreases considerably, especially in the case of Ring 5, but it recovers immediately behind the rings and is approximately constant over the downstream portion. The lengths of sepatation bubbles in front of and rear of the rings were estimated by oil film method: in the case of Ring 2.5, about 6 mm and 18 mm, and in the case of Ring 5, about 10 mm and 60 mm, respectively.

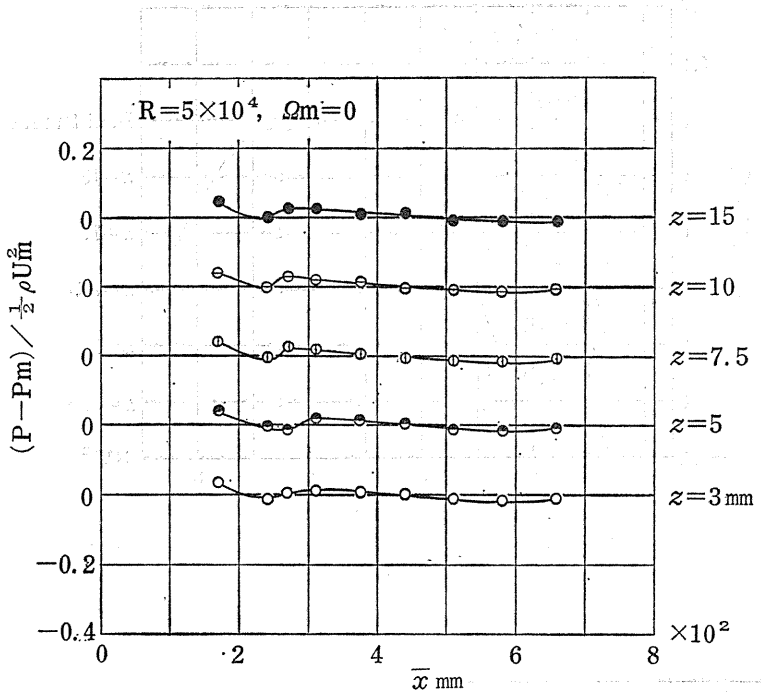

Fig. 3. 5. Pressure distribution in the case of Ring 2.5.

In Fig. 3. 7 velocity profiles for Ring 5 in the range from $\bar{x}=310$ mm to 657 mm at $\Omega_m=0$ are presented. The velocity distribution at the station of $\bar{x}=310$ mm which is 67.5 mm downstream from the rear surface of the ring shows the profile which is usually found in reattached boundary layer. It is seen from the figure that the velocity profiles approach the ordinary pattern without disturbance but does not recover the similar shape as shown in Fig. 3. 3.

Peculiar profiles measured at the station of $\bar{x}=270$ mm in the case of Ring 5 when $\Omega_m=1$ and 2 are shown in Fig. 3. 8. Reverse flow near the wall is appreciable in the axial velocity distribution and the velocity component in the peripheral direction has a remarkable shape which has a maximum value at $z\fallingdotseq 8$ mm. This phenomenon might be explained as follows. Fluid particles close to the cylinder surface obtain great peripheral velocities in the upstream portion of the ring. Under the influence of the ring, the velocities become greater in the peripheral direction through a "no-slip" condition at the outer ring edge. The boundary layer separates again and reattaches to the cylinder surface, thus developing a new boundary layer there. Comparison of the profiles of $\Omega_m=1$ and 2 suggests that the separation bubble behind the ring diminishes with increasing speed ratio.

Figure 3. 9 shows the velocity distribution over the range from $\bar{x}=310$ mm to

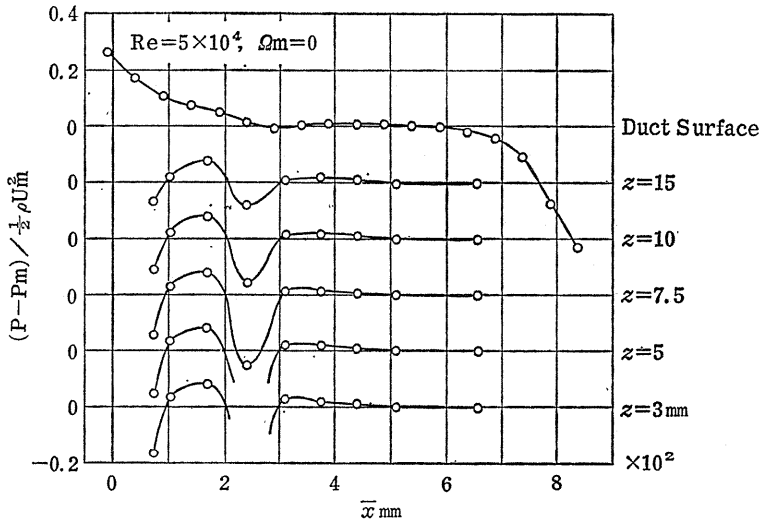

Fig. 3. 6. Pressure distribution in the case of Ring 5.

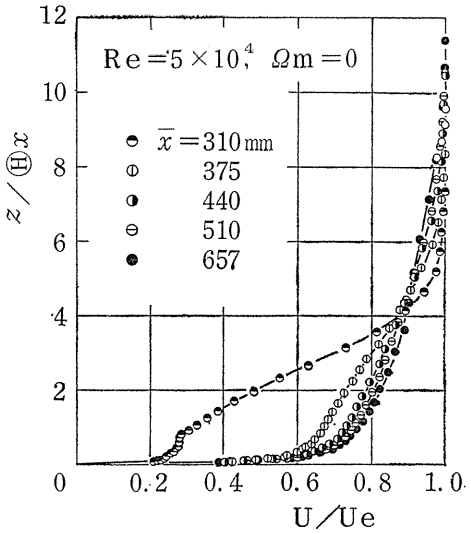

Fig. 3. 7. Velocity profiles of reattached flow for Ring 5 at $\Omega_m=0$.

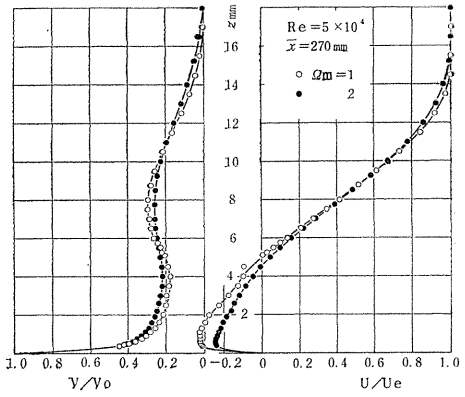

Fig. 3. 8. Velocity profiles at the station of $\bar{x}=270$ mm for Ring 5.

657 mm when $\Omega_m=2$. Separated boundary layer reattaches to the wall at the section of $\bar{x}=310$ mm, then gradually recovers to the normally developed profiles. In contrast with the large deformation of axial velocity profiles, the change in the profiles of peripheral velocity component is relatively small and limited near the

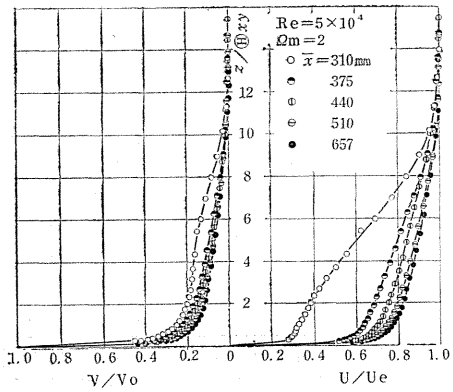

Fig. 3. 9. Velocity profiles for Ring 5 at $\Omega_m=2$.

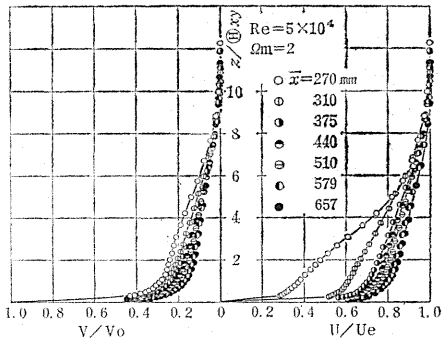

Fig. 3. 10. Velocity profiles for Ring 2.5 at $\Omega_m=2$.

ring as seen in these figures. It may be said that the velocity distribution exhibits more stability in the peripheral direction than in the axial direction.

In Fig. 3. 10 the velocity profiles for Ring 2.5 at $\Omega_m=2$ are presented. The boundary layer is reattached to the wall at the station of $\bar{x}=270$ mm. The variation of velocity profiles toward downstream gives the same feature as that for Ring 5.

3. 4. 3. The case of Step

Another method to produce disturbance in the boundary layer employed in these

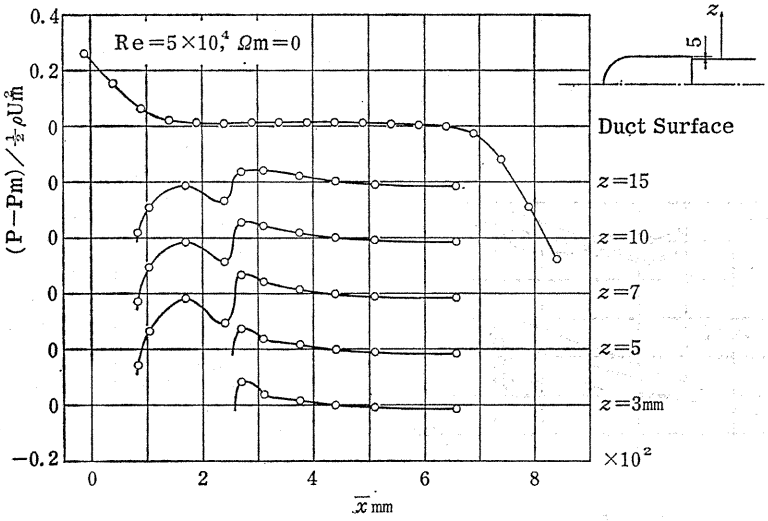

Fig. 3. 11. Pressure distribution in the case of Step.

experiments is to set a backward facing step of 5 mm height at the same place where the rings were placed.

Measured pressure distribution in the case of stationary body is presented in Fig. 3. 11. The pressure change occurring at the step has a tendency which is somewhat different from that existing in the case of Ring 5. Passing the ring, pressure increases steeply, and remains approximately constant in the downstream region; also it rises immediately behind the step but slightly decreases in the downstream direction as seen in Fig. 3. 11. The length of separation bubble behind the step was estimated at about 23 mm by oil film method; this is considerably shorter than that of Ring 5.

Figure 3. 12 shows the velocity distribution on the body spinning at $\Omega_m=2$. As in the cases of Ring 5 and Ring 2.5, change in the peripheral velocity profiles is smaller than that of axial direction. Moreover it can be seen that the axial velocity profiles in this case exhibit less deformation than in the case of Ring 5 and this phenomenon may be ascribed to the relatively small separation bubble and slight favorable pressure gradient as mentioned above.

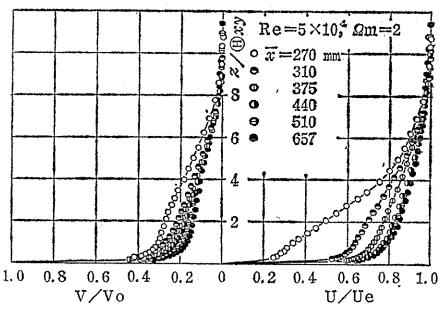

Fig. 3. 12. Velocity profiles for Step at $\Omega_m=2$.

3. 4. 4. Momentum thicknesses

Since we usually express the development of boundary layers using integrated thicknesses, some values of momentum thicknesses of these flows are presented in Figs. 3. 13 - 3. 16. The values of Θ_x of Ring 2.5 and Ring 5 exhibit strong effect of disturbance by showing sudden enlargement behind the rings, as seen in Figs. 3. 13 and 3. 14. The developments of Θ_{xy} of Cylinder and of Ring 2.5 and Ring 5 are, except in the region immediately behind the rings, similar and they take the same values approximately as presented in Figs. 3. 15 and 3. 16. Spatial stability of the perpheral velocity distribution to the disturbance can explain this character.

There are some methods of calculation for momentum thicknesses of turbulent boundary layer on a spinning body in axial stream[3), 48)], but none of them take

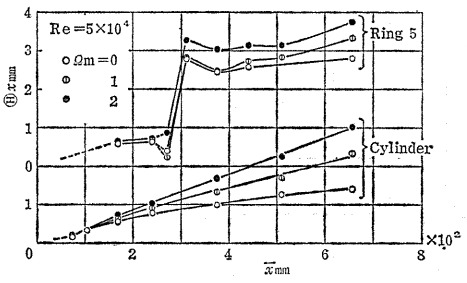

Fig. 3. 13. Developments of momentum thickness θ_x for Cylinder and Ring 5.

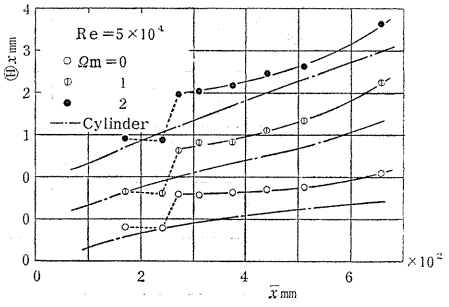

Fig. 3. 14. Developments of momentum thickness θ_x for Ring 2.5.

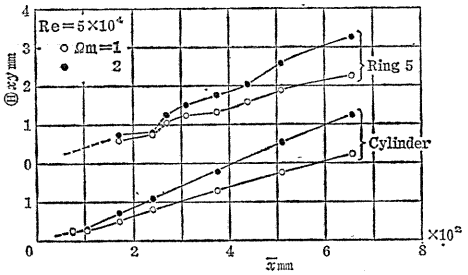

Fig. 3. 15. Developments of angular momentum thickness θ_{xy} for Cylinder and Ring 5.

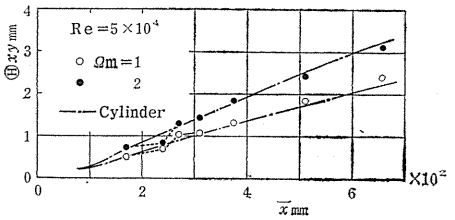

Fig. 3. 16. Developments of angular momentum thickness θ_{xy} for Ring 2.5.

account of the effect of curvature. Thus we can not compare the experimental values of θ_x and θ_{xy} with any theory.

3. 5. Relationship between axial and peripheral velocity components

Polar plots of velocity vector proved its utility to explore the characteristics of the skewed boundary layer. According to the experimental results obtained by the authors[4], the following equation is well satisfied in the most turbulent boundary layers:

$$1-U/U_e=V/V_0. \tag{3.7}$$

An implication of this equation is realized if we take the coordinate moving with the body that is, if the Eq. (3.7) holds, then the relative velocity vectors at various heights from the body surface in such a frame are coplanar and it can be said that the boundary layer is quasi-two-dimensional. Since the plane containing the relative vector is tangent to the relative velocity on the spinning cylinder in uniform inviscid axial stream, it is questionable to apply Eq. (3.7) to the present problem of thick skewed boundary layer.

Extension of the concept of quasi-collaterality may be obtained by the following argument. Let the cylinder rotates in inviscid flow and take a coordinate fixed to the cylinder in which ξ_1 is the relative main flow direction at radius r and ξ_2 is the peripheral direction, as shown in Fig. 3. 17a, so the frame is rotating non-orthogonal. The magnitude of relative velocity U_R at radius r is

$$U_R=\sqrt{U_e^2+(r\omega)^2}. \tag{3.8}$$

The coordinate surface made by ξ_1 and r axes is a spiral surface.

Let U_{rel} be the relative velocity in the boundary layer, its components in ξ_1-and ξ_2-directions in this coordinate are

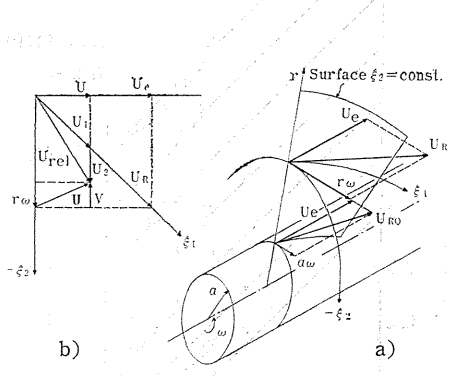

Fig. 3. 17.
a) Rotating non-orthogonal frame.
b) Relationship between various velocity components.

$$\left.\begin{aligned} U_1 &= U_R U/U_e, \\ U_2 &= V - r\omega(1-U/U_e), \end{aligned}\right\} \tag{3.9}$$

respectively, as seen from Fig. 3. 17 b. If the velocity vector in the boundary layer is tangent to the spiral surface of ξ_1 and r then we call the velocity distribution is quasi-collateral in a generalized sense and the condition which must be satisfied in this case is obviously $U_2=0$ and yields

$$1-U/U_e = aV/rV_0. \tag{3.10}$$

Equation (3. 10) reduces to Eq. (3. 7) when the boundary layer is thin compared with the cylinder radius. In what follows we use the term quasi-collateral in the meaning of Eq. (3. 10). The term quasi-collateral may not be appropriate in this case but it is retained for apparent reasons.

A diagram of polar plots taking the ordinate as aV/rV_0 and the abscissa as U/U_e is used to compare the measured velocity distribution with Eq. (3. 10). Measured points fall on the line if the quasi-collateral condition is satisfied. Of many experimental results, the typical two figures, that is, the polar plots of Cylinder and Ring 5 when $\Omega_m=2$, will be shown here; the others are presented in Refs. 49) and 50).

Figure 3. 18 corresponds to the case of Cylinder. The boundary layer still remains laminar at the section of $\bar{x}=74$ mm and it has quasi-collateral profile,

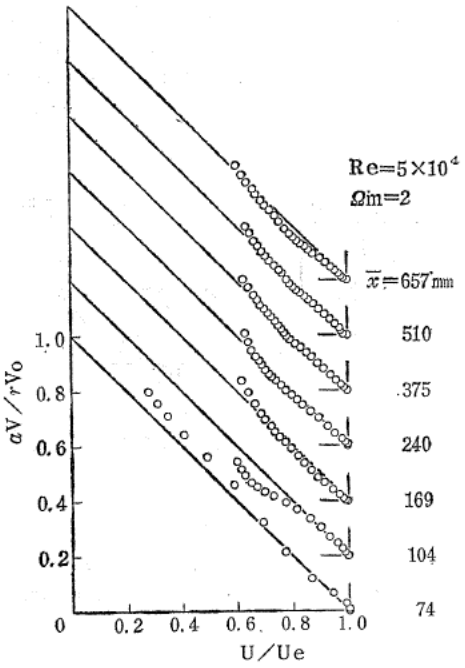

Fig. 3. 18. Polar plots of velocity distribution for Cylinder.

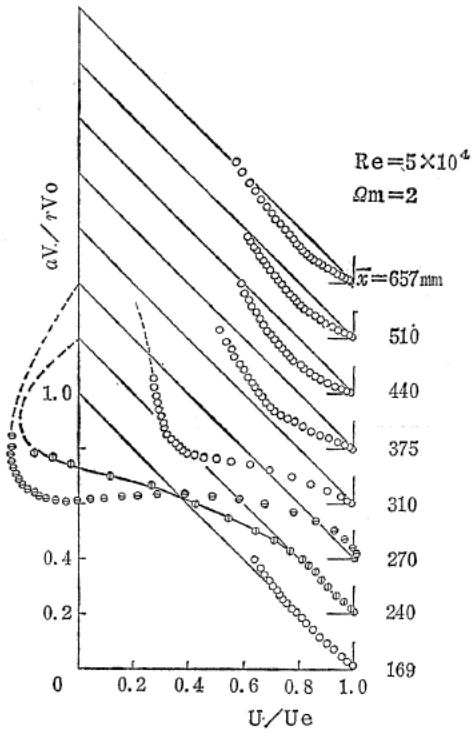

Fig. 3. 19. Polar plots of velocity distribution for Ring 5.

while the corresponding plots for $\Omega_m=1$ has deviated from this condition. The variation of the velocity distribution of laminar flows in this region with speed ratio can be explained by considering the centrifugal acceleration produced at the nose part[4]. At $\bar{x}=104$ mm the transition is occurring and the polar plots show the effect of the upstream portion. But a fully turbulent boundary layer in the range from $\bar{x}=240$ mm to 657 mm satisfies the relationship of Eq. (3. 10) reasonably well.

The polar plots of Ring 5 at $\Omega_m=2$ are shown in Fig. 3. 19. A quasi-collateral velocity distribution exists at $\bar{x}=169$ mm in front of the ring and there the boundary layer is turbulent. The section of $\bar{x}=240$ mm is the front surface of the ring. The section of $\bar{x}=270$ mm is in the separated bubble region; the x-component of the velocity distribution exhibits a reverse flow, and at $\bar{x}=310$ mm the boundary layer reattaches to the wall. It is clearly seen from this figure that quasi-collateral turbulent boundary layer upstream of the ring is greatly disturbed by the ring and it deviates from the quasi-collateral condition. After passing the ring the boundary layer recovers the quasi-collateral profile. In these experiments, however, the velocity profile does not satisfy the quasi-collaterality even at the most downstream station.

Turning now to the appearance of the disturbance by the ring, it may be inferred that the deviation of velocity distribution from the quasi-collateral condition at the ring would be provoked partly by the Coriolis force in the ξ_2-direction, adding to the retardation of axial velocity.

Of course the degree of deviation from the quasi-collaterality is varied according to the type of roughness element, speed ratio and others. From these figures the deviation of velocity distribution from this condition is clearly seen intuitively, but it is desirable to define a suitable parameter to express the change of the deviation along the current length. It may be reasonable to suppose a thickness which relates to angular momentum produced by U_2 defined by Eq. (3. 9) can serve for the purpose. Also a displacement thickness Δ_1 produced by velocity component U_1 is able to exclude the effect of the total boundary layer thickness. So we will define a shape parameter H_{22} as follows:

$$H_{22}=\frac{\theta_{22}}{\Delta_1}=\int_a^{r_\delta}\left(\frac{U_2}{V_0}\right)^2\frac{r}{a}dr\Big/\int_a^{r_\delta}\left(1-\frac{U_1}{U_R}\right)\frac{r}{a}dr. \qquad (3.11)$$

The developments of the shape parameters with axial distance for various kinds of rotating bodies at $\Omega_m=2$ are shown in Fig. 3. 20. This parameter is almost zero for Cylinder in all measuring stations corresponding to the quasi-collateral distribution. An extreme peak value of this parameter appears at $\bar{x}=270$ mm in the case of Ring 5 and it decreases rapidly downstream. The cases of Ring 2. 5 and Step show approximately the same peak value but the reduction of the parameter is slightly more rapid in the case of Step than in the case of Ring 2. 5.

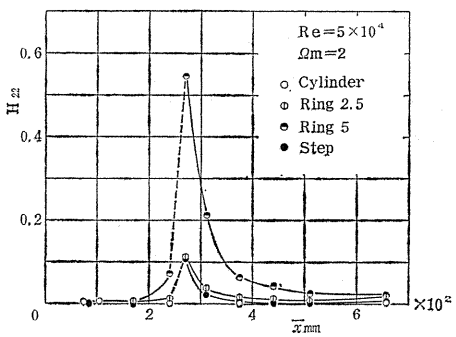

Fig. 3. 20. Variation of shape parameter H_{22} at $\Omega_m=2$.

The comparison between the results of two speed ratios in these experiments has shown that the shape parameters have larger values and reduce more slowly in the case of smaller speed ratio than in the case of higher speed ratio[49].

Consulting the polar plots and the change in the shape parameters, including when $\Omega_m=1$, it might be deduced that this parameter is fairly suitable one in describing the deviation of the velocity distribution from the quasi-collateral condition irrespectively of the type of disturbance and speed ratio within these experiments.

3. 6. Concluding remarks

Experiments were carried out to explore the turbulent boundary layers which developed on a cylinder, on the cylinders with two kinds of rings and on the cylinder with a step, rotating in axial flow. Detailed results of mean flow measurements are presented. Some features clarified by this study may be summarized as follows:

First, the definition of momentum thicknesses require the consideration of curvature when the total thickness of the boundary layer reaches about 20% of the cylinder radius. The rotation promotes the effect of the curvature.

Second, the disturbance generated by a ring or a step affects on the axial velocity profiles stronger than on the peripheral velocity profiles.

Third, the changes in the boundary layer produced by a roughness element are analyzed using a generalized quasi-collateral condition. A shape parameter introduced is able to show the recovery of the velocity distribution to the quasi-collateral form in the downstream.

Ⅳ Experiments on the Thick Turbulent Boundary Layers on a Rotating Cylinder under Pressure Gradients

4. 1. Introduction

In a previous chapter, we described the experiments on the effect of a single roughness element on the flow structure in the turbulent boundary layer on a rotating cylinder.

This chapter presents an investigation about the relatively thick turbulent boundary layers on a cylinder spinning in axial flows with pressure gradients; the influence of pressure gradient, as well as a roughness element, is an important factor affecting the turbulent boundary layer. Firstly, descriptions are given of mean velocity profiles measured in the turbulent boundary layers affected by adverse and favorable pressure gradients. Next, similarity considerations of these flows are made. That is, the distribution of peripheral shear stresses in the boundary layer is calculated numerically from measured mean velocity profiles, and on the basis of their near wall behaviors a formula for a logarithmic velocity distribution in the peripheral direction is deduced; this expression is different from that for a two-dimensional turbulent boundary layer on a flat plate. It is shown that the expression deduced succeeds in depicting the measured velocity profiles. Furthermore, a Richardson number that has been proposed as a parameter describing the turbulence character in such destabilized flow is examined.

Bissonnette & Mellor[6] and Lohmann[7] have investigated the similar flow to the present one. But both their experiments were made using a cylinder model

which consisted of two parts: a stationary section followed by a spinning afterbody. The flow fields generated therein which are subjected to a disturbance due to a sudden circumferential strain is rather different from that of the present experiments.

4. 2. Experimental apparatus and procedures

The wind tunnel employed is the same one as used in the experiments in Chapter Ⅲ. Experiments have been carried out in three turbulent boundary layers on a circular cylinder rotating in the pressure gradient fields generated by means of a tapered sleeve inserted in the tunnel. The experimental arrangements and the measuring stations are shown in Fig. 4. 1. In this figure, cases (Ⅰ) and (Ⅱ) are the setups of the rotating bodies of 200 mm and 140 mm diameters, respectively, in the flow fields of the adverse pressure gradients, and case (Ⅲ) is the same rotating body as in case (Ⅱ) but in the favorable pressure gradient field. In what follows,

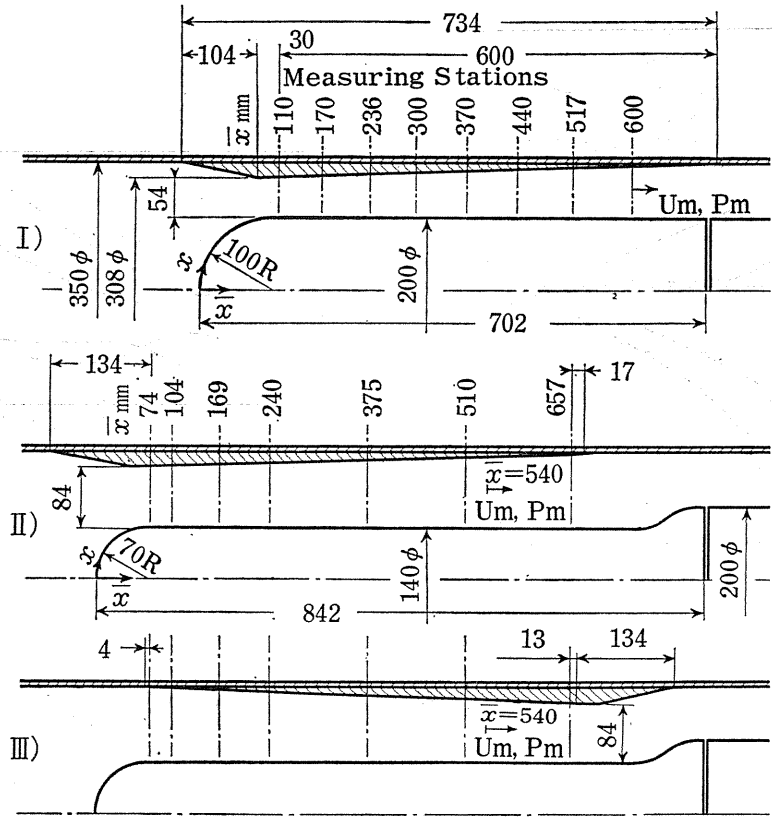

Fig. 4. 1. Experimental arrangements and measuring stations.

use is made of the designations of AP(Ⅰ), AP(Ⅱ) and FP for cases (Ⅰ), (Ⅱ) and (Ⅲ) respectively. The experimental results with nearly constant pressure in the previous chapter are cited as CP here. The taper-angle of the sleeve has been determined such as not to induce the boundary layer separation on the inner surface of the sleeve. In the case of AP(Ⅰ), the value of Reynolds number Re is fixed at 8×10^4, and the speed ratio Ω_m is varied: 0, 0.65, 1, 1.5, 2 and 2.5. For the other cases, the experimental conditions are the same as in Chapter Ⅲ. The present chapter is concerned mainly with the experimental results at $\Omega_m=0$, 1 and 2, especially at $\Omega_m=2$.

4. 3. *Experimental results*

The static-pressure distribution at $z=0$ mm for AP(Ⅰ) and $z=3$ mm for the others when the bodies are at rest is shown in Fig. 4. 2. Each gradient of the curves is nearly constant except in the region where the nose effect exists, and is not so steep as to induce separation or relaminarization. The distribution of Clauser's equilibrium shape factor G, which is defined in a two-dimensional turbulent boundary layer, is presented in Fig. 4. 3. The figure shows that the adverse pressure gradients affect this shape factor more than the favorable pressure gradient does.

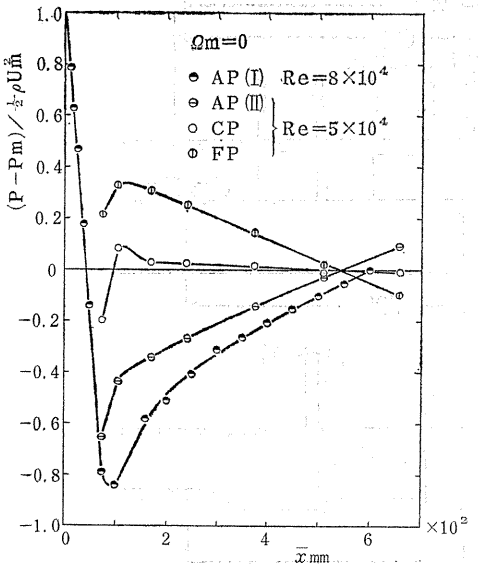

Fig. 4. 2. Static-pressure distribution.

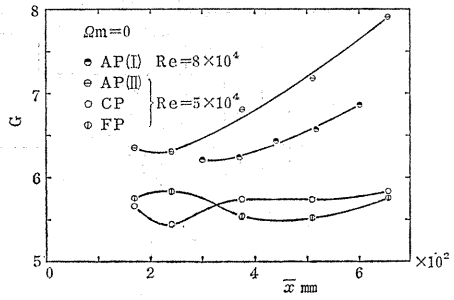

Fig. 4. 3. Distribution of shape factor

$$G=\int_0^\delta\{(U_e-U)^2/U_\tau^2\}dz\Big/\int_0^\delta\{(U_e-U)/U_\tau\}dz.$$

Axial and peripheral velocity profiles in the turbulent boundary layers for AP(Ⅱ) and FP at $\Omega_m=2$ are presented in Figs. 4. 4 and 4. 5, respectively. In the case of AP(Ⅱ), the axial velocity profiles are nearly similar; this result is in contrast with non-similar profiles for CP in the previous experiments. The adverse pressure gradient in the present experiments is acting as a compensation for the acceleration effect owing to the rotation, so that the axial profiles have good similarity. The profiles for FP are not similar in both components.

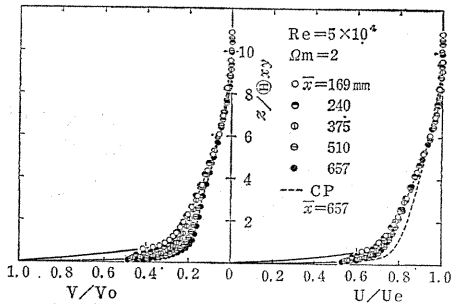

Fig. 4. 4. Velocity profiles in the turbulent boundary layer for AP(Ⅱ) at $\Omega_m=2$.

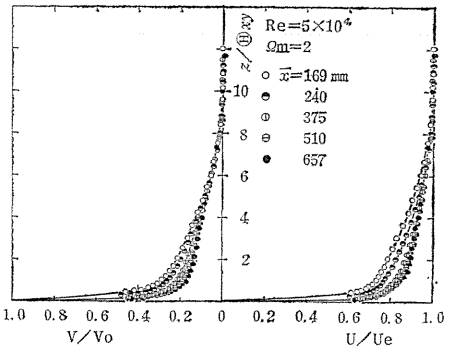

Fig. 4. 5. Velocity profiles in the turbulent boundary layer for FP at $\Omega_m=2$.

The velocity profiles at the upstream and the downstream stations for AP(Ⅱ) and FP are shown in Fig. 4. 6, solid curves being for CP. The axial profiles in the three turbulent boundary layers, which nearly coincide at the upstream station, deviate considerably from one another at the downstream station due to the effects of the pressure gradients. On the other hand the peripheral profiles nearly coincide with one another at the downstream station as well as at the upstream station.

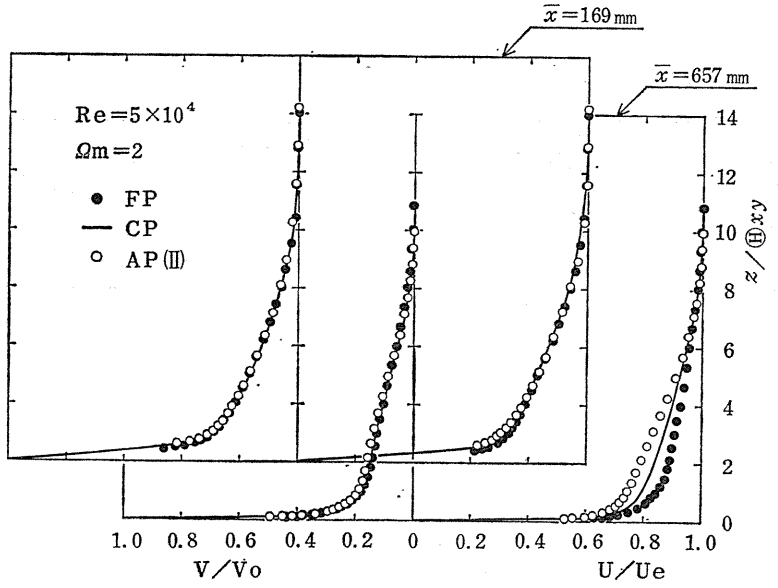

Fig. 4. 6. Comparison between velocity profiles for FP, CP and AP(Ⅱ).

These features indicate that there is almost no effect of pressure gradients on the peripheral velocity components within the limits of these experiments.

Figure 4. 7 shows the polar plots of the velocity distribution compared with the extended quasi-collateral condition given in the previous chapter. At the station of $\bar{x}=169$ mm, which is taken to be most upstream for the fully developed turbulent flows in these experiments, the polar plots for AP(Ⅱ) and FP satisfy fairly well the condition of the quasi-collaterality, but the deviations from this condition appear downstream. These deviations are attributed mainly to the changes in the axial velocity profiles because of the pressure gradients. That is, the distribution for AP(Ⅱ) shifts to the deceleration side and that for FP does to the acceleration side.

The developments of integrated thicknesses, θ_x and θ_{xy}, are shown in Figs. 4. 8 and 4. 9 respectively. It is obvious that the pressure gradients affect θ_{xy} less sensitively than θ_x, and this character may also be attributed to the stability of peripheral velocity distribution.

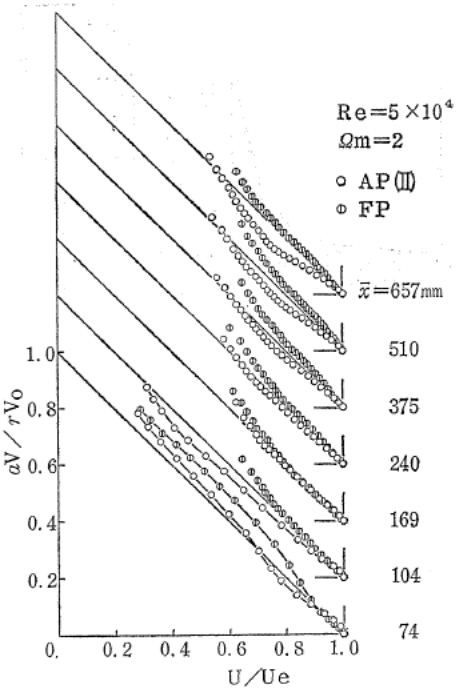

Fig. 4. 7. Polar plots of velocity distribution for AP(Ⅱ) and FP.

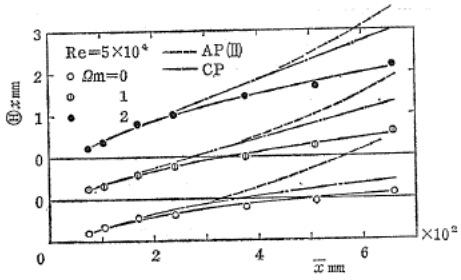

Fig. 4. 8. Developments of momentum thickness θ_x. Experimental points represent the case of FP.

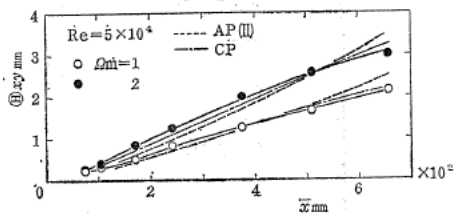

Fig. 4. 9. Developments of angular momentum thickness θ_{xy}. Experimental points represent the case of FP.

4. 4. The character of the turbulent boundary layer

4. 4. 1. Shear-stress distribution in the layer

Shear-stress distribution, especially near the wall, is important in relation to the law of the wall in a turbulent boundary layer. Here the peripheral shear-stress distribution is examined, because the experimental results described above show the

insensitivity of the peripheral velocity profiles to the effect of the external pressure gradients. The peripheral shear-stress component is obtained as

$$\tau_y=\rho V_0^2\partial_x\left\{-\frac{1}{\Omega}\left(\frac{a}{r}\right)^2\int_r^\delta\frac{U}{U_e}\frac{V}{V_0}\left(\frac{r}{a}\right)^2dr\right\}-\rho V_0V\partial_x\left(\frac{1}{\Omega}\frac{a}{r}\int_a^r\frac{U}{U_e}\frac{r}{a}dr\right), \quad (4.1)$$

through integration of the third equation of Eq. (3.1). Introducing the values of measured mean velocities into Eq. (4.1), τ_y can be calculated numerically. Calculated values of τ_y and $r^2\tau_y$ made dimensionless with reference to those values on the wall are shown in Figs. 4. 10 and 4. 11, after the curves have been made

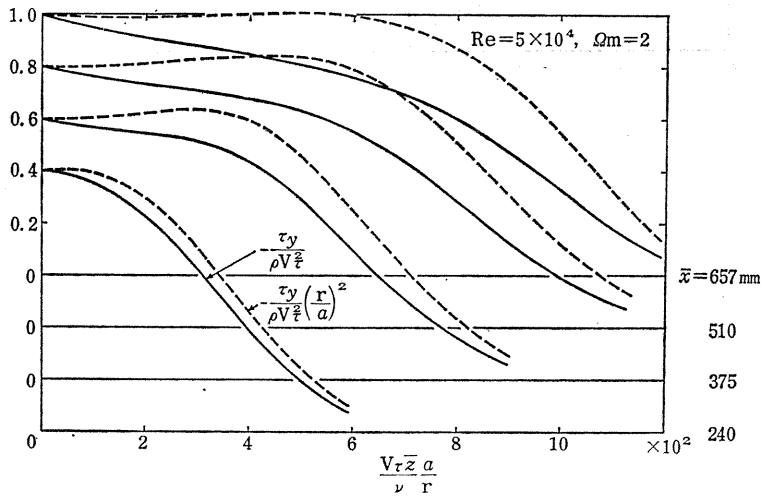

Fig. 4. 10. Distribution of peripheral shear stresses in the turbulent boundary layer for CP.

smooth. The abscissa is a wall variable appearing in an expression for the logarithmic velocity distribution as seen in the next section. These figures show that a region of $r^2\tau_y=$const. exists near the wall rather than that of $\tau_y=$const. corresponding to the flat plate flow.

This feature is also confirmed from the basic equation as follows. When we consider the proximity of the wall, it may be possible to neglect the inertia terms on the left hand side in the basic equation in the peripheral direction. Hence we obtain

$$\partial_r(r^2\tau_y)/\rho r^2=0, \quad (4.2)$$

whence follows

$$r^2\tau_y=a^2\tau_{0y}=\text{const.} \quad (4.3)$$

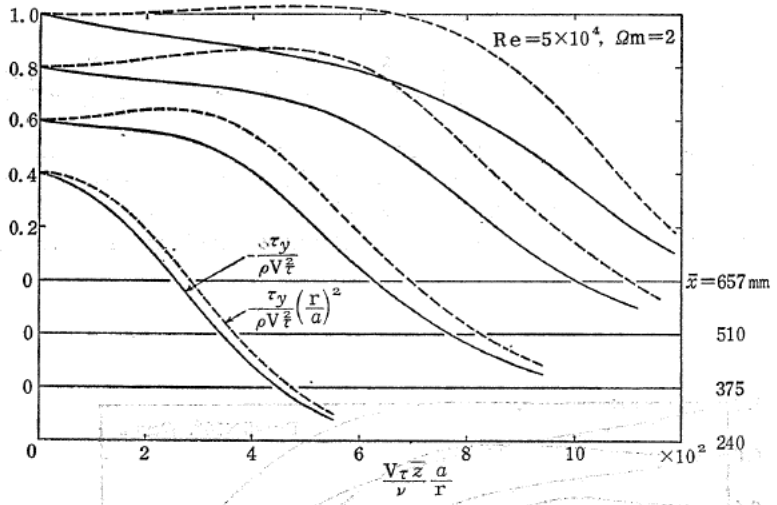

Fig. 4. 11. Distribution of peripheral shear stresses in the turbulent boundary layer for AP(Ⅱ).

This equation states the existence of a layer where the moment of the peripheral shear force per unit depth at radius r is constant. This layer is equivalent to the constant-stress layer in the turbulent boundary layer on a flat plate.

4. 4. 2. Universal velocity distribution in the turbulent boundary layer

As to the mean velocity distribution in the turbulent boundary layer on a flat plate, a similarity law holds independently of Reynolds number for the first approximation. In particular the logarithmic velocity distribution law is, as well known, applied in a region near the wall with and without external pressure gradients. This formula is possibly applicable to the flow on a stationary cylinder, if the boundary-layer thickness is so small in comparison with the radius of the cylinder that the transverse curvature effect is negligible. However, when the thickness is comparable with the radius of the cylinder, many authors have discussed what type of the law of the wall must apply in the turbulent boundary layer affected by the transverse curvature. These considerations are relevant to the problem of the turbulent boundary layer on a rotating cylinder, and a brief description of them is given as under for reference.

Two typical proposals among them are as follows:

Richmond[51] : $$U/U_\tau = A\log_{10}\{(U_\tau z/\nu)(1+z/2a)\}+B, \tag{4.4}$$

Rao[44] : $$U/U_\tau = A\log_{10}\{(U_\tau a/\nu)\ln(r/a)\}+B, \tag{4.5}$$

where A and B are empirical constants for the flat-plate flow. Equation (4.4) has been obtained by an application of Coles' streamline hypothesis to an axisym-

metric flow. On the ther hand, Rao has derived Eq. (4.5) on the basis of the velocity distribution in a sublayer where the axial shear force per unit depth of a cylinder surface at radius r is constant. He has concluded that this formula depicts much experimental data including those of Richmond better than Eq. (4.4) does. Both the equations reduce to the expression for the flat-plate flow as $a \to \infty$.

Willmarth & Yang[52] and Bissonnette et al.[6] have applied Eq. (4.4) to their experimental data, and some papers[53],[54] on numerical studies have made use of Eq. (4.5). Chase[55] has recommended Rao's hypothesis, not only because Eq. (4.5) represents quite well the experimental data, but also because the mean velocity distribution in the wall layer on a thin cylinder is expressed by a single function: $U/U_\tau = F\{(U_\tau a/\nu)\ln(r/a)\}$, including the exact velocity profile in the sublayer. On the contrary, Bradshaw & Patel[56] pointed out an uncertainty in the basis of Rao's argument and threw doubt on any law of the wall analysis itself in the case where z/a is large. Nevertheless, for not extremely large values of z/a, they derived from the so-called mixing-length formula a logarithmic expression different from both Eqs. (4.4) and (4.5). However, this equation differs little from Eq. (4.5) numerically over a wide range of z/a. Therefore, Eq. (4.5) in which the wall variable $(U_\tau a/\nu)\ln(r/a)$ is naturally included is utilized to express the present experimental data on a stationary cylinder. Although Rao & Keshavan[57] have suggested in their later experiments that the values of A and B in this equation vary with Reynolds numbers, in this report Sarnecki's constant values for the flat-plate flow are used.

The experimental values for AP(Ⅱ), CP and FP arranged by Eq. (4.5) are presented in Fig. 4. 12, where U_τ is determined from the so-called Clauser chart based on this expression. The scale numbers on the ordinate in the figure correspond to the experimental values for CP. The effects of the pressure gradients are perceptible in outer regions, but Eq. (4.5) describes the measured profiles very well. However, whether or not there is an advantage in Rao's hypothesis is not completely concluded here, because the values of δ/a in these cases are relatively small, i. e., 0. 3 at most.

Turning now to the problem on a universal velocity distribution in the skewed turbulent boundary layer on a rotating circular cylinder, a few considerations have been made. The turbulence in the boundary layer is affected by the rotation of the cylinder and the mean velocity profiles also have different forms from those with no rotation. These features can be examined from the consideration of a universal velocity distribution. In authors' earlier study[4], a logarithmic velocity distribution for the peripheral flow on a rotating conical body was deduced in the same expression as that for a two-dimensional turbulent flow. That formula has succeeded in describing the measured peripheral profiles. However, the comparison of the peripheral velocity profiles in the present experiments with the Clauser chart based on this expression showed that there was no definite linear portion of the measured profiles; this formula is not suitable for the thick turbulent boundary layers. In this section, a consideration is made of the peripheral velocity distribution, as a contribution to the clarification of a universal velocity distribution law valid in this turbulent boundary layer.

The universal law of the wall which might be expected to hold near the wall in a turbulent boundary layer states that the mean velocity distribution in this region is completely determined only by local physical quantities. We may expect the main parameters governing the peripheral flow to be τ_{0y}, V, V_0, a, r, ρ and μ.

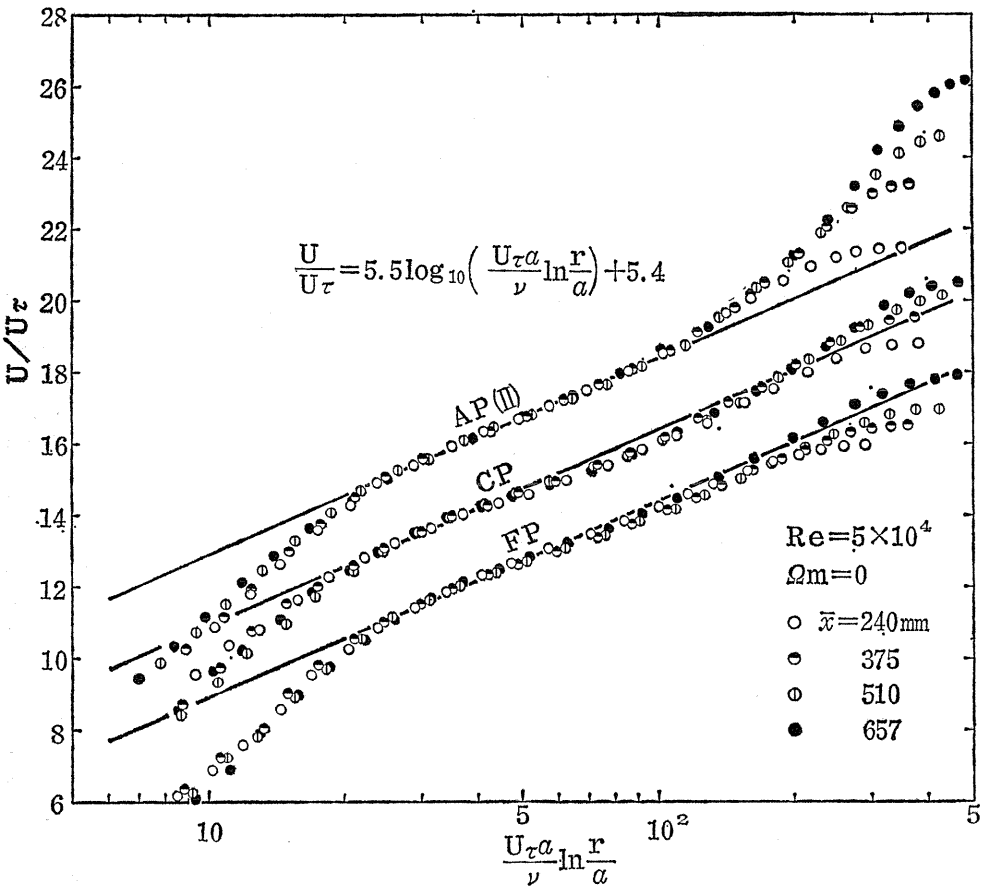

Fig. 4. 12. Logarithmic velocity distribution in the boundary layer with no rotation.

The measured velocity profiles show that there is no effect of τ_{0x} for the first approximation. Therefore, a general relation of the law of the wall is written in a functional form

$$V/V_\tau=f(V_\tau a/\nu,\ r/a,\ V_0/V_\tau). \tag{4.6}$$

We deduce its actual form more legitimately than Rao[44] did, who conjectured the law of the wall in axisymmetric flow on a stationary cylinder from the velocity distribution in the sublayer.

Near the wall there exists the region where Eq. (4.3) is valid. Substitution of the second equation in Eq. (3.3) into Eq. (4.3) yields

$$(\nu r^3/a^3V_\tau)\partial_r(aV/rV_\tau)-r^2\overline{vw}/a^2V_\tau^2=1. \tag{4.7}$$

Dimensional coefficient $\nu r^3/a^3V_\tau$ can be absorbed in a new dimensionless variable z^+ defined by the following equation,

$$\partial_r z^+=V_\tau a^3/\nu r^3. \tag{4.8}$$

Then Eq. (4.7) is transformed into

$$\partial_{z^+}(aV/rV_\tau)-r^2\overline{vw}/a^2V_\tau^2=1. \tag{4.9}$$

Implicit assumption deriving Eq. (4.3) is that we can neglect the variation of flow condition in the axial direction if we limit the consideration near the wall. So it may be legitimate to expect the solution of Eq. (4.9) has a form:

$$aV/rV_\tau=F(z^+). \tag{4.10}$$

Putting $z^+=0$ at $r=a$, then integration of Eq. (4.8) yields

$$z^+=(V_\tau a/\nu)(r^2-a^2)/2r^2. \tag{4.11}$$

Above consideration shows that z^+ is a relevant wall variable in description of various quantities near the wall concerned only in the peripheral direction. Let $a\to\infty$ with fixed z, then $z^+\to V_\tau z/\nu$, which was used in our previous paper[4]. At the cylinder wall $V=V_0$, so we obtain $V_0/V_\tau=F(0)$. We seek the correspondence between the law of the wall in the flat-plate flow and that of the peripheral direction in this flow. Let

$$f(z^+)=F(0)-F(z^+), \tag{4.12}$$

and then

$$aV/rV_\tau=F(0)-f(z^+), \tag{4.13}$$

that is,

$$\{V_0-(a/r)V\}/V_\tau=f(z^+). \tag{4.14}$$

This is the law of the wall that we looked for. Since in the viscous sublayer Reynolds stresses may be negligible, we obtain from Eq. (4.9)

$$\{V_0-(a/r)V\}/V_\tau=z^+. \tag{4.15}$$

This is an equation corresponding to the linear profile of the sublayer in flat-plate flow.

Now we research the universal velocity distribution law in the viscosity negligible region which is still in the wall layer, using a matching method according to Millikan[58]. For the purpose, we must establish the law to which the velocity in the outer region obeys. If it is permissible in the outer region to consider the peripheral velocity is also independent of the axial component, governing parameters in the region are τ_{0y}, V, a, r, δ and ρ. Then dimensional reasoning defines a relationship:

$$V/V_\tau=g(r/a,\ \delta/a). \tag{4.16}$$

This equation is an equivalence of the defect law in some sense, so we may call it simply "defect law" without leading to confusion in this problem. If we assume the existence of the overlap region where both the law of the wall (4.14) and the defect law (4.16) are valid, then in that region we have

$$f[(V_\tau a/\nu)\{(r/a)^2-1\}/2(r/a)^2]+(a/r)g(r/a,\ \delta/a)=V_0/V_\tau. \tag{4.17}$$

Generally speaking, V_0/V_τ is a function of $V_\tau a/\nu$ and δ/a, so if we put $V_\tau a/\nu=\xi$, $r/a=\eta$, $\delta/a=\zeta$ and $V_0/V_\tau=h(\xi, \zeta)$, Eq. (4.17) is rewritten

$$f[\xi(\eta^2-1)/2\eta^2]+g(\eta, \zeta)/\eta=h(\xi, \zeta). \tag{4.18}$$

Differentiating Eq. (4.18) by ξ and η respectively and comparing the results, we obtain

$$\xi\partial_\xi h(\xi, \zeta)=-\{\eta(\eta^2-1)/2\}\partial_\eta\{g(\eta, \zeta)/\eta\}, \tag{4.19}$$

which can hold only if either term is equal to a function of ζ only, $A(\zeta)$ say. Thus,

$$\left.\begin{aligned}\partial_\xi h(\xi, \zeta)&=A(\zeta)/\xi,\\ \partial_\eta\{g(\eta, \zeta)/\eta\}&=-2A(\zeta)/\eta(\eta^2-1),\end{aligned}\right\} \tag{4.20}$$

and

$$df/dz^+=A(\zeta)/z^+. \tag{4.21}$$

Equation (4.21) shows that $A(\zeta)$ must be a constant, A say, and the universal velocity distribution in the overlap region expressed by the wall variable z^+ is

$$f(z^+)=\{V_0-(a/r)V\}/V_\tau=A\ln z^++C_2, \tag{4.22}$$

where C_2 is a constant of integration. Using the common logarithms and turning the variable z^+ to the intelligible one, Eq. (4.22) can be rewritten

$$\left.\begin{aligned}\{V_0-(a/r)V\}/V_\tau&=C_1\log_{10}\{(V_\tau\bar{z}/\nu)(a/r)\}+C_2,\\ \text{where}\qquad \bar{z}&=(r^2-a^2)/2r.\end{aligned}\right\} \tag{4.23}$$

The variable $\bar{z}$ has an evident geometrical meaning.

From Eq. (4.20) we obtain

$$h(\xi, \zeta)=A\ln\xi+B(\zeta), \tag{4.24}$$

and

$$g(\eta, \zeta)/\eta=A\ln\{2\eta^2/(\eta^2-1)\}+B(\zeta)-C_2, \tag{4.25}$$

where $B(\zeta)$ is the constant of integration dependent on ζ. The latter equation is a concrete form of the defect law in that region.

Equation (4.23) is equivalent to the well-known universal logarithmic velocity distribution for the flat-plate flow.

Measured profiles arranged on the basis of this formula are given in Figs. 4.13 and 4.14, where V_τ is estimated from Eq. (4.1). These figures show the existence of a linear portion expressed in Eq. (4.23); the logarithmic velocity distribution obtained succeeds in describing the peripheral profile in the thick turbulent boundary layer on a rotating cylinder, and the wall variable $(V_\tau\bar{z}/\nu)(a/r)$ is relevant.

The validity of Eq. (4.16) on which the formula of the logarithmic velocity distribution is based is verified as follows. An example of velocity profiles according to the usual expression of defect law without the effect of transverse curvature

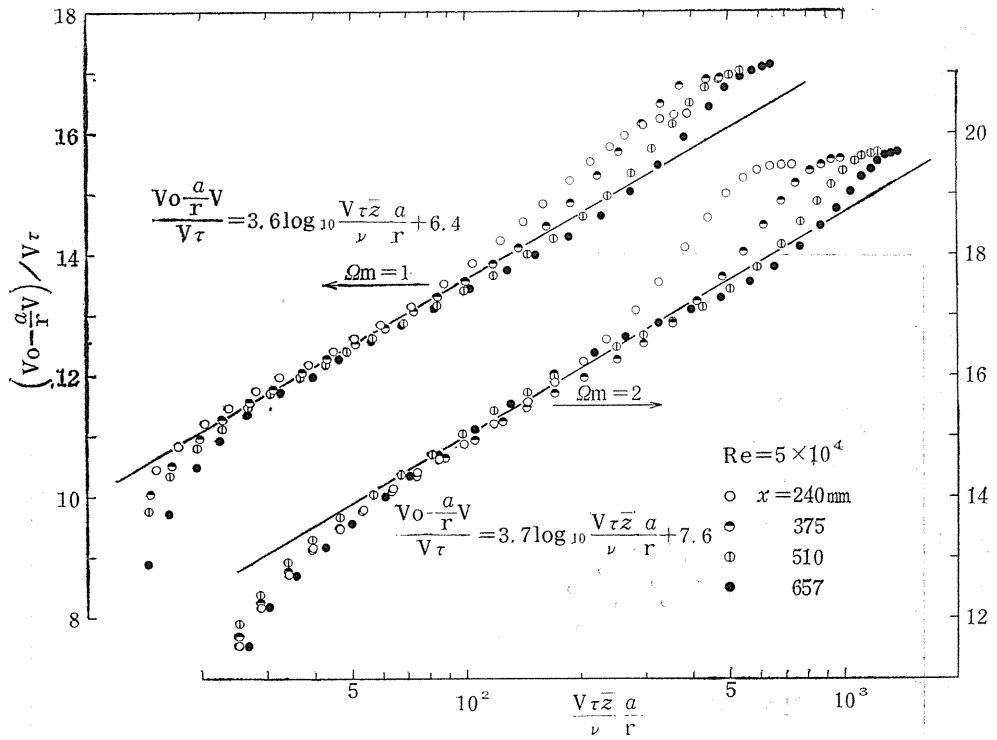

Fig. 4. 13. Logarithmic plots of peripheral velocity profiles for CP on the basis of Eq. (4. 23).

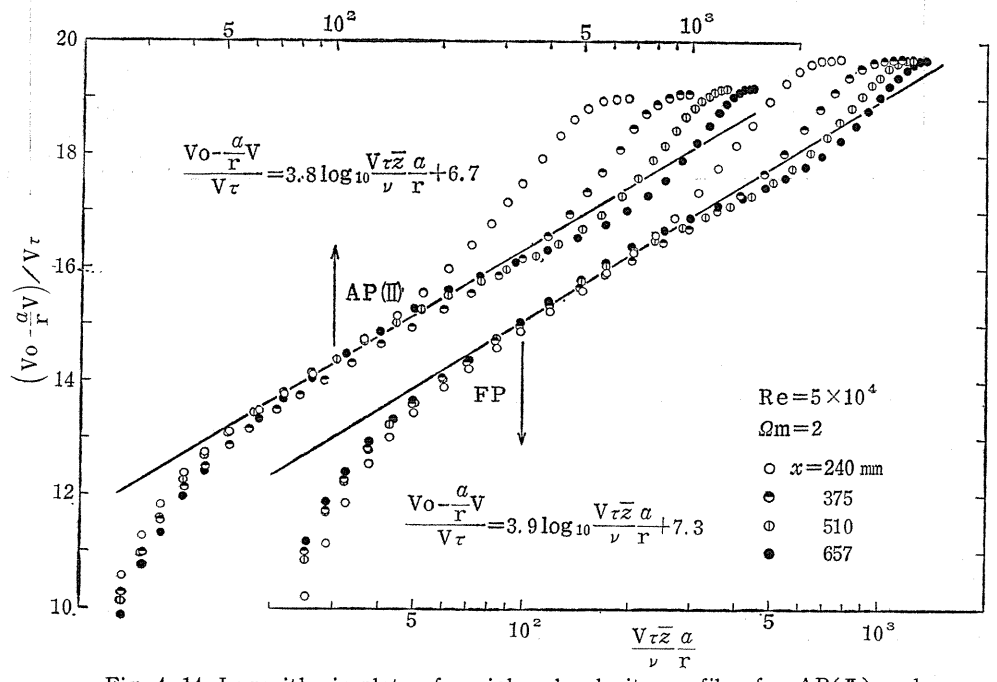

Fig. 4. 14. Logarithmic plots of peripheral velocity profiles for AP(Ⅱ) and for FP on the basis of Eq. (4. 23).

is given in Fig. 4. 15. As illustrated, the experimental values do not fall on a single curve, and the usual defect law for the flat-plate flow is invalid. In Fig. 4. 16 measured profiles represented on the basis of the defect law (4. 16) with the curvature effect are shown. It can be concluded that the defect law (4. 16) is varid for this peripheral flow, although the data compared with one another in this figure are restricted because this equation is a funtion of two variables.

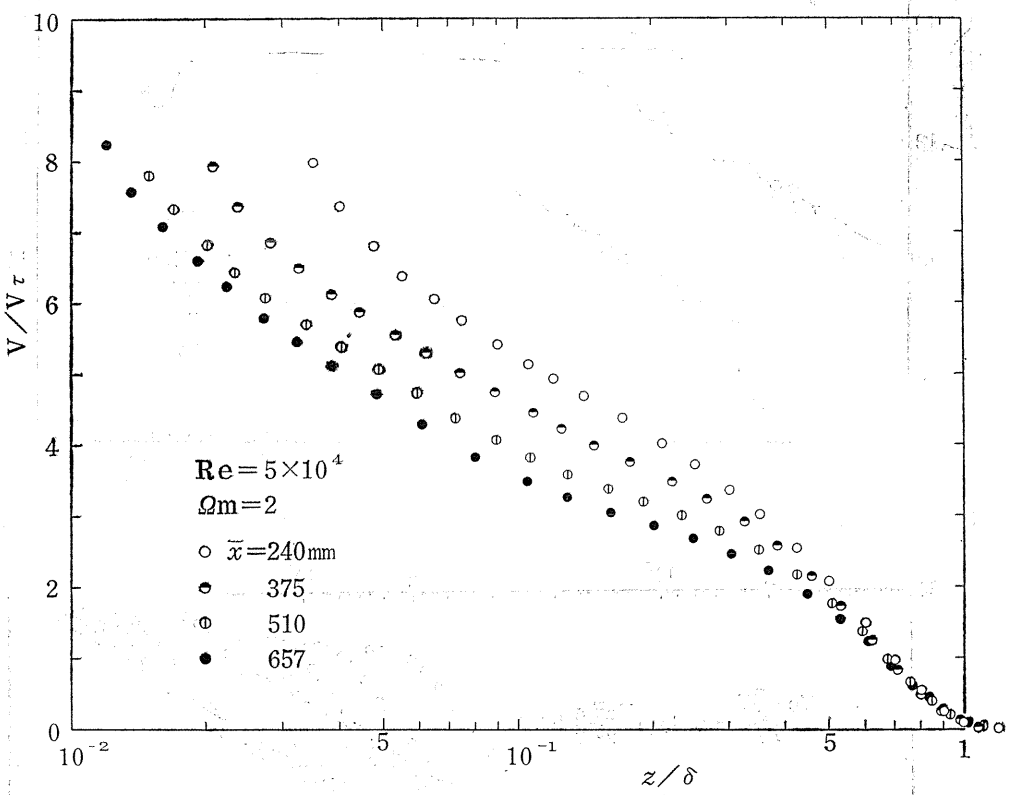

Fig. 4. 15. Logarithmic plots of peripheral velocity profiles for CP on the basis of the velocity-defect law in two-dimensional turbulent boundary layer.

Although the peripheral velocity distribution is characterized by the logarithmic form expressed by Eq. (4. 23), there is a problem that C_1 and C_2 in this equation so far considered to be constant are not exactly constant. The solid lines in Figs. 4. 13 and 4. 14 are drawn such as to be in accord with the measured values under the same experimental conditions, in relation to a Richardson number given in the next section. The value of C_1 is different from that for the two-dimensional logarithmic velocity distribution but is roughly constant within the present experiments, whereas the value of C_2 varies considerably. These features may be investigated in connection unlike the dimensional analysis as employed above. Hence, in the first place, it is to be desired that the physical significances of C_1 and C_2 be clarified.

Using the eddy kinematic viscosity ε, the equation for the peripheral shear

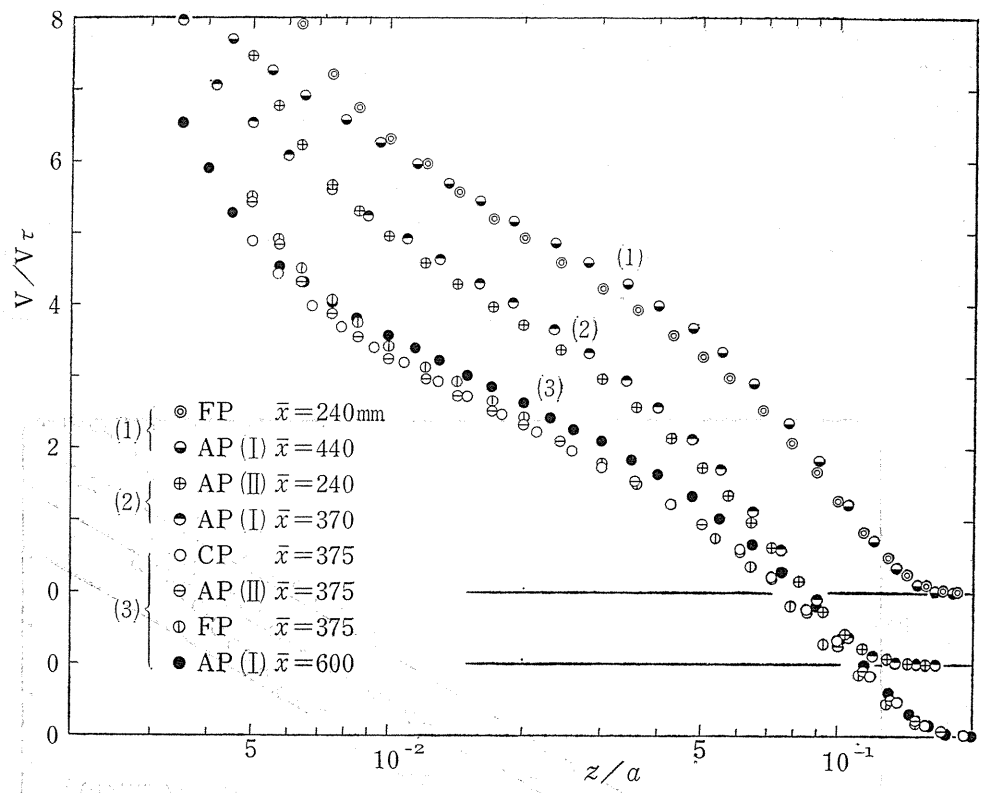

Fig. 4. 16. Logarithmic plots of peripheral velocity profiles in the turbulent boundary layers on the basis of the defect law (4. 16) : (1) $\Omega_m=2$, $\delta/a\fallingdotseq 0.156$, (2) $\Omega_m=2$, $\delta/a\fallingdotseq 0.124$, (3) $\Omega_m=1$, $\delta/a\fallingdotseq 0.165$.

stress is rewritten

$$\tau_y=\rho\varepsilon(\partial_r V-V/r). \tag{4.26}$$

Assuming a length scale to be $\bar{z}a/r$ appearing in the wall variable, we obtain

$$\varepsilon=\kappa V_\tau \bar{z}a/r, \tag{4.27}$$

where κ is an empirical constant. The validity of Eq. (4.27) has been found using the calculated values of τ_y. The value of κ has been in the range from 0.6 to 0.7, unlike the Kármán constant. Substituting Eqs. (4.3) and (4.27) into Eq. (4.26), and through integration, we obtain

$$(a/r)V=-(V_\tau/\kappa)(\ln\bar{z}a/r+C), \tag{4.28}$$

where C is a constant of integration that should be determined from the condition at the other edge of the sublayer. Equation (4.28) corresponds to Eq. (4.22), but further assumptions are needed for reducing the former to the latter. However, from the comparison between these equations, it becomes evident that $A=1/\kappa$ or $C_1=(1/\kappa)\ln 10$, and that C_2 depends on κ and on the condition of the sublayer.

Although C_1 and C_2 have the same meanings as those in the flat-plate flow, in order to elucidate their distinction it is desirable to make further experiments under various conditions. Nevertheless, as $a \to \infty$, Eq. (4.23) should tend to the equation for the flat-plate flow. Therefore, these fearures of C_1 and C_2 seem to be owing to the effect of the curvature; this effect is discussed in relation to the Richardson number in the next section.

Bissonnette et al.[6] have also dealt with the problem of the transverse curvature effect on the flow in a logarithmic region. Their argument is complicated and does not have so simple a meaning as in this research. It is difficult to compare the two cases. Instead, an example of their measured profiles rearranged on the basis of Eq. (4. 23) is given in Fig. 4. 17, where V_τ is determined from experimental

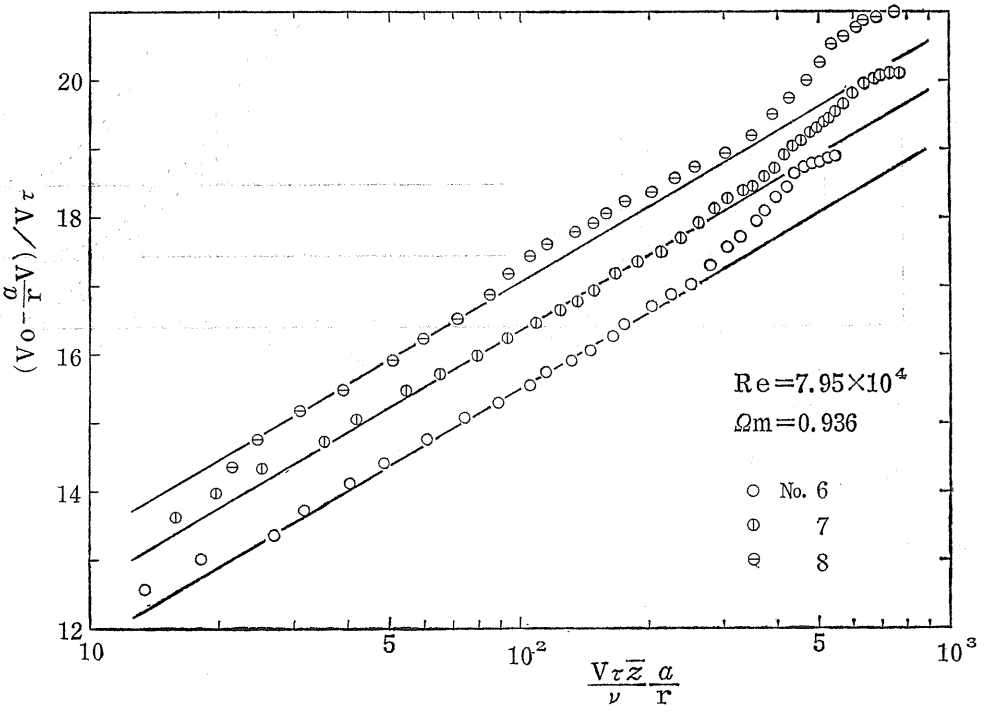

Fig. 4. 17. Logarithmic plots of peripheral velocity profiles measured by Bissonnette & Mellor[6] on the basis of Eq. (4. 23) : the value of C_1 in Eq. (4. 23) is 3. 7.

values obtained using a hot-wire anemometer. There exist the linear portions expressed in Eq. (4. 23) and their gradients are nearly equal to those of the present experiments. But the profiles do not fall on a single line; this is probably because of unreliability of V_τ determined by means of a hot-wire anemometer and because of the unusual condition of the sublayer caused by the peculiarity of the boundary layer flow as mentioned in section 4. 1. Bissonnette et al. have mentioned nothing about the sublayer.

4. 4. 3. Effect of the rotation on the turbulent boundary layer

The flow in the turbulent boundary layer on a rotating body is affected by the destabilizing centrifugal force. According to Bradshaw[13], who showed that the effect of rotation or streamline curvature on a turbulent flow is expressed by parameters analogous to the Richardson number in meteorology, an appropriate Richardson number can be considered as the ratio of the square of the Brunt-Väisälä frequency ω_{BV} to the square of the turbulent frequency. Thus Cham & Head[48] have given the analogous Richardson number for the flow on a rotating cylinder as

$$Ri=(2V/r^2)\{\partial_r(rV)\}/(\partial_r U_{rel})^2, \tag{4.29}$$

where U_{rel} is the mean velocity in a frame rotating with the cylinder. Cham et al. simplified Eq. (4.29) extremely on the assumptions that the boundary layer is so thin as to be $r/a=1$ and that the velocity profile is quasi-collateral. However, their assumptions are invalid in the present experiments, where the boundary layer is not very thin. For example, using a typical one of the measured velocity profiles that satisfies fairly well the quasi-collateral condition, the minimum value of R_i calculated from the simplified expression is five or six times as small as that from Eq. (4.29). Hence, Eq. (4.29) is used here itself as a convenient parameter.

The calculated values of R_i using the experimental data for CP and AP(Ⅱ) are presented in Figs. 4. 18 and 4. 19. R_i is always negative, that is, the flow is subjected to the destabilizing effect, and it can be expected that the turbulent

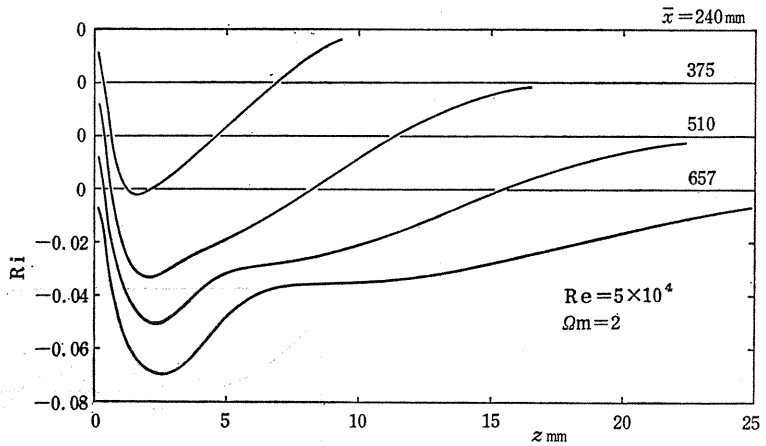

Fig. 4. 18. Distribution of Richardson number in the turbulent boundary layer for CP.

mixing is increased. This parameter tends to decrease downstream.

In this report, the concern is with the region where the logarithmic velocity distribution describes well the real velocity profiles. The comparison of the profiles

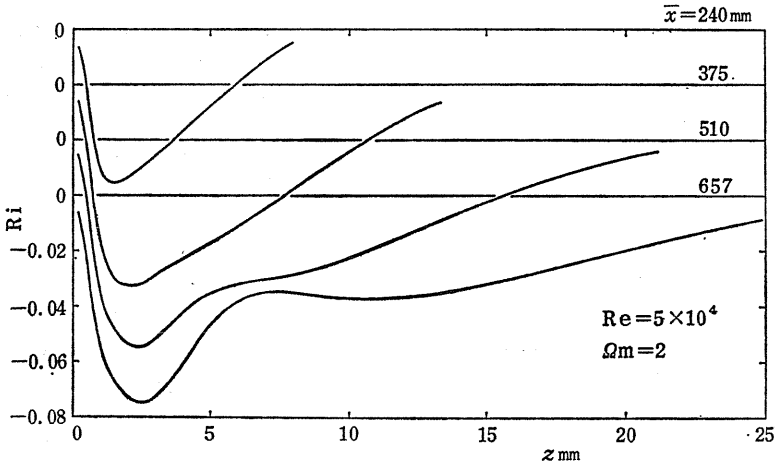

Fig. 4. 19. Distribution of Richardson number in the turbulent boundary layer for AP(Ⅱ).

of R_i with measured velocity profiles represented by Eq. (4. 23) indicates that the logarithmic region coincides roughly with the region where R_i takes the minimum value. The same was also true for the other cases in these experiments. Therefore, its minimum value Ri_{min} can be possibly regarded as a representative one. Thus the value of C_1 in Eq. (4. 23) which has so far been somewhat arbitrary is definitely determined from the several experimental points in that region. In order to examine the effect of R_i on the logarithmic region, the value of C_1 obtained above at each station of $\bar{x}$ in the present experiments including for CP is plotted in terms of Ri_{min} in Fig. 4. 20. The scatter is somewhat large but C_1 is effectively constant in the range of the present experimental conditions. Since the Richardson number tends to zero as $a \to \infty$, it can be expected that C_1 tends to the value 5. 5 for the flat-plate flow as $Ri_{min} \to 0$.

The variation of mixing length l is expressed, for example, by the Monin-Oboukhov formula

$$1-\beta Ri = l/l_0$$

where β is a positive coefficient which varies from one flow situation to another and the suffix '0' represents the flat-plate flow (in what follows, the same is used). The Monin-Oboukhov formula here is possibly rewritten

$$1-\beta Ri_{min} = l/l_0 \sim C_{10}/C_1$$

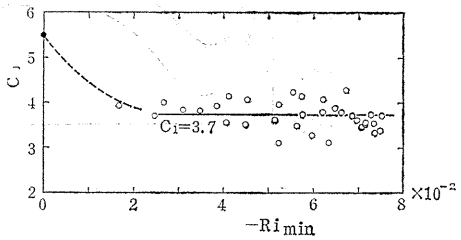

Fig. 4. 20. Change in the value of C_1 in Eq. (4. 23) in terms of the minimum value of Richardson number.

by use of the representative Ri_{min} instead of R_i. Therefore, the constancy of C_1 indicates that βRi_{min} is approximately constant.

In curved flows, the rate of mixing-length variation normal to the solid boundary is reasonably estimated from the ratio of the energy determined from ω_{BV} to the turbulent energy of fluctuating component normal to the wall. Hence the change in the mixing length becomes

$$1-l/l_0 \sim \omega_{BV}^2/(\overline{w}^2/l_0^2).$$

On the other hand, we have

$$Ri \sim \omega_{BV}^2/(\overline{u}^2/l_0^2),$$

from the physical meaning of R_i by Cham et al. Thus we obtain

$$\beta \sim \overline{u}^2/\overline{w}^2$$

through the Monin-Oboukhov formula. It can be considered that an increase in $|Ri_{min}|$ is tends to make the turbulence near the wall isotropic, that is, the value of β decreases because of an increase in $\overline{w}^2$ with Ω_m. Therefore, the value of βRi_{min} becomes constant irrespective of the variation of Ri_{min} within the limits of these experiments.

Hughes & Horlock[59] have also discussed the change in the mixing length in connection with the conservation of the momentum of fluid. The expression deduced, however, turns out to be essentially the same as the Monin-Oboukhov formula.

The effect of R_i on C_2 in Eq. (4. 23) is presumable since the sublayer may be affected by the instability. Variation of C_2 with Ri_{min} is presented in Fig. 4. 21. As illustrated, C_2 is likely to increase with a decrease in Ri_{min}, but this result is somewhat unreliable since the value of C_2 depends heavily on the accuracy of V_τ. Nevertheless, C_2 tends surely to the value 5.4 of the flat-plate flow as $Ri_{min} \to 0$.

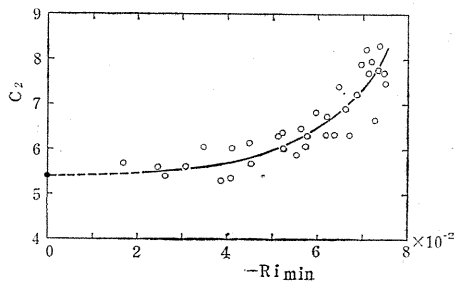

Fig. 4. 21. Change in the value of C_2 in Eq. (4. 23) in terms of the minimum value of Richardson number.

4. 5. *Concluding remarks*

On the basis of the mean flow measurements and discussion on the turbulent boundary layers about a rotating cylinder, the following conclusions can be made:

First, mean velocity profiles in the peripheral direction are insensitive to the influence of the pressure gradients in comparison with those in the axial direction. The profiles in the polar diagram tend to deviate to the acceleration side or to the deceleration side, according as the boundary layer undergoes the effect of the favorable or the adverse pressure gradient.

Second, distribution of the peripheral shear-stresses in the turbulent boundary layer has been calculated from the measured velocity profiles. The result shows

the existence of a layer near the wall where the moment of the peripheral shear force per unit depth at radius r is constant, and not the existence of the so-called constant-stress layer in the flat-plate flow; this feature can also be deduced from the basic equation.

Third, the similarity considerations for the peripheral flow near the wall have been made, on the basis of the dimensional reasoning and of the near wall behavior of the shear-stress profile, then a logarithmic velocity distribution law has been obtained using the matching method. This formula succeeds in depicting the measured peripheral profiles in these turbulent boundary layers.

Forth, distribution of Richardson number, i. e., one of the parameters describing the effect of instability, indicates that its minimum value Ri_{min} is a representative one in the logarithmic region. The changes in C_1 and C_2 in the logarithmic formula in terms of Ri_{min} show that the former is effectively constant within the limits of the present experiments and the latter tends to increase with a decrease in Ri_{min}.

References

1) Wieselsberger, C., Physikalische Zeitschrift, Bd. **28** (1927), 84.
2) Schlichting, H., Ing.-Arch., Bd. **21** (1953), 227.
3) Parr, O., Ing.-Arch., Bd. **32** (1963), 393.
4) Furuya, Y. & Nakamtra, I., Trans. ASME, Ser. E, Vol. **37** (1970), 17.
5) Cham, T-S. & Head, M. R., Aeron. Quart., Vol. **22** (1971), 389.
6) Bissonnette, L. R. & Mellor, G. L., J. Fluid Mech., Vol. **63** (1974), 369.
7) Lohmann, R. P., Trans. ASME, Ser. I, Vol. **98** (1976), 354.
8) Koosinlin, M. L., Launder, B. E. & Sharma, B. I., Trans. ASME, Ser. C, Vol. **96** (1974), 204.
9) Koosinlin, M. L. & Lockwood, F. C., AIAA J., Vol. **12** (1974), 547.
10) Sharma, B. I., AIAA J., Vol. **15** (1977), 271.
11) Launder, B. E., Priddin, C. H. & Sharma, B. I., Trans. ASME, Ser. I, Vol. **99** (1977), 231.
12) Koosinlin, M. L. & Lockwood, F. C., Trans. ASME, Ser. I, Vol. **96** (1974), 303.
13) Bradshaw, P., J. Fluid Mech., Vol. **36** (1969), 177.
14) Hannah, D. M., A. R. C. R. & M., No. **2772** (1947).
15) Rittmann, K., Ing.-Arch., Bd. **38** (1969), 304.
16) Muraca, R. J., Ph. D. Thesis, Virginia Polytechnic Inst., Virginia, (1970).
17) Illingworth, C. R., Phil. Mag., Vol. **44** (1953), 389.
18) Illingworth, C. R., Phil. Mag., Vol. **45** (1954), 1.
19) Wadhwa, Y. D., Phil. Mag., Vol. 3, No. **26** (1958), 152.
20) Barbett, K. E., J. Fluid Mech., Vol. **27** (1967), 779.
21) Fox, J., NASA TN. D-**2491**, (1964).
22) Dorfman, L. A. & Serazedinov, A., Int. J. Heat & Mass Transf., Vol. 8 (1965), 317.
23) Banks, W. H. H., ZAMP, Vol. **16** (1965), 780.
24) Manohar, R., ZAMP, Vol. **18** (1967), 320.
25) Seban, R. A. & Bond, R., J. Aeron. Sci., Vol. **18** (1951), 671.
26) Glauert, M. B. & Lighthill, M. J., Proc. Roy. Soc. Lond., Ser. A, Vol. **230** (1955), 188.
27) Stewartson, K., Quart. Appl. Math., Vol. **13** (1955), 113.
28) Sakiadis, B. C., A. I. Ch. E. J., Vol. **7** (1961), 467.
29) Yasuhara, M., J. Aeros. Sci., Vol. **29** (1962), 667.
30) Jaffe, N. A. & Okamura, T. T., ZAMP, Vol. **19** (1968), 564.

31) Van Dyke, M., Problems of Hydrodynamics and Continuum Mechanics, Publ. SIAM, (1969), 748.
32) Gersten, K. & Gross, J. F., Int. J. Heat & Mass Transf., Vol. **16** (1973), 2241.
33) Nakamura, I., Research Bulletin of Dept. of General Education, Nagoya Univ., Vol. **16** (1972), 31.
34) Nachtsheim, P. R. & Swigert, P., NASA TN. D-**3004**, (1965).
35) Hoskin, N. E., 50 Jahre Grenzschichtforschung, ed. Görtler, H. & Tollmien, W., Fieder Vieweg und Sohn, (1955), 127.
36) Tomotika, S. & Imai, I., Rept. Aero. Res. Int. Tokyo, No. **13** (1938), 389.
37) Luthander, S. & Rydberg, A., Physikalische Zeitschrift, Bd. **36** (1935), 552.
38) Dorfman, L. A., Hydrodynamic Resistance and the Heat Loss of Rotating Solids, Oliver & Boid, (1963).
39) Kreith, F., Convection Heat Transfer in Rotating Systems in Advances in Heat Transfer, Vol. 5, Academic Press, (1968).
40) Howarth, L., Phil. Mag., Vol. **42** (1951), 1308.
41) Stewartson, K., Proc. Symp. Boundary layer Res., Int. Union Theoret. Appl. Mech. Freiburg i. Br., (1957), 59.
42) Singh, S. N., Phys. Fluids, Vol. **13** (1970), 2452.
43) Rogers, M. H. & Lance, G. N., J. Fluid Mech., Vol. **7** (1960), 617.
44) Rao, G. N. V., Trans. ASME, Ser. E, Vol. **34** (1967), 237.
45) Hinze, J. O., Turbulence, 2nd Ed., McGraw-Hill, (1975), 588.
46) Moore, F. K., Three-Dimensional Boundary Layer Theory, Advances in Applied Mechanics, Vol. 4, ed. Dryden, H. L. & von Kármán, T., Academic Press, (1956).
47) Preston, J. H., J. Fluid Mech., Vol. **3** (1957), 373.
48) Cham, T-S. & Head, M. R., J. Fluid Mech., Vol. **42** (1970), 1.
49) Nakamura, I., Yamashita, S. & Furuya, Y., Proc. 2nd Int. JSME Symp., Fluid Machinery and Fluidics, Tokyo, Vol. **2**, (1972), 41.
50) Furuya, Y., Nakamura, I., & Yamashita, S., Proc. 5th Conf. Fluid Machinery, Budapest, Vol. **1**, (1975), 297.
51) Richmond, R. L., Ph. D. Thesis, Calif. Inst. Tech., Calif., (1957).
52) Willmarth, W. W. & Yang, C. S., J. Fluid Mech., Vol. **41** (1970), 47.
53) Cebeci, T., Trans. ASME, Ser. D, Vol. **92** (1970), 545.
54) White, F. M., Trans. ASME, Ser. D, Vol. **94** (1972), 200.
55) Chase, D. M., AIAA J., Vol. **10** (1972), 849.
56) Bradshaw, P. & Patel, V. C., AIAA J. Vol. **11** (1973), 893.
57) Rao, G. N. V. & Keshavan, N. R., Trans. ASME Ser. E, Vol. **39** (1972), 25.
58) Millikan, C. B., Proc. 5th Intern. Congr. Appl. Mech., Cambridge, USA, (1939), 386.
59) Hughes D. W. & Horlock, J. H., Proc. Symp. Internal Flows, (Inst. Mech. Engr.), (1971), B 78.

Nomenclature

x : meridian coordinate; distance measured along the meridian curve of the body from the foward stagnation point.
$\bar{x}$: axial coordinate; axial distance from the foward stagnation point.
y : azimuthal angle.
z : distance from the body surface.
R : radius of the body, $R=R(x)$.
r : radial distance from the axis of revolution.
a : radius of the cylinder.
δ : boundary layer thickness.
r_δ : radius of the outer edge of the boundary layer.

ω : angular velocity of the rotating body.
U, V, W : mean velocity components in the x-, y-, and z-directions respectively.
u, v, w : fluctuating velocity components in the x-, y-, and z-directions respectively.
P : mean static pressure.
P_m : reference mean static pressure.
U_m : reference main stream velocity.
U_e : local main stream velocity.
R_m : reference radius of the body.
a_m : reference radius of the cylinder.
V_w : peripheral velocity of the body surface in Chap. II.
V_o : peripheral velocity of the cylinder surface in Chaps. III and IV.
R_e : Reynolds number$=U_mR_m/\nu$ or U_ma_m/ν.
Ω : speed ratio$=R_m\omega/U_m$. In Chaps. III and IV it designates local speed ratio V_o/U_e.
Ω_m : reference speed ratio in Chaps. III and IV$=a_m\omega/U_m$.
τ_x, τ_y : shearing stress components in the x-, and y-directions respectively.
U_τ, V_τ : friction velocity components in the x-, and y-directions respectivety.
Δ_x : displacement thickness of the thick boundary layer; Eqs. (2. 74) and (3. 5a).
θ_x : momentum thickness of the thick boundary layer; Eqs. (2. 74) and (3. 5a).
θ_{xy} : angular momentum thickness of the thick boundary layer; Eqs. (2. 75) and (3. 5a).
θ_{yy} : integrated thickness which shows the variation of pressure in the boundary layer due to the rotation; Eqs. (2. 75) and (3. 5a).
$\theta'_\tau, \theta'_{\tau\tau}, \theta'_{yy}$: integrated thicknesses determined by the fluctuating velocities; Eq. (3. 5b).
G : Clauser's equilibrium shape factor $=\int_0^\delta\{(U_e-U)^2/U_\tau{}^2\}dz \Big/ \int_0^\delta\{(U_e-U)/U_\tau\}dz$.
H_{22} : shape factor of the velocity profile in the polar plot; Eq. (3. 11).
R_i : Richardson number; Eq. (4. 29).